MULLARD LIMITED
Mullard House
Torrington Place
London, W.C.1

CONTENTS

Effect of Reverse Recovery Time of Thyristors on Efficiency of Parallel Inverters 230-232

Line Timebase to Scan the A28-13W 233-235

Equalising the Performances of Small Permanent Magnet D.C. Motors 236-238

Recent Advances in Germanium Microwave Mixer Diodes 239-248

Equivalent Circuit and Frequency Response Characteristic of the Bandpass Filter comprising Two Coupled Tuned Circuits 249-255

Design of a High-power u.h.f. Trebler 256-260

VOL. 8 No. 78 NOVEMBER 1965

Mullard Technical Communications

VOLUME 8 NUMBER 78

November 1965

Mullard

Mullard Technical Communications

VOLUME 8 NUMBER 78 November 1965

Contents

Effect of Reverse Recovery Time of Thyristors on Efficiency of Parallel Inverters *K. H. Williamson* 230

Line Timebase to Scan the A28-13W *D. Skelton* 233

Equalising the Performances of Small Permanent Magnet D.C. Motors *J. Catherall* 236

Recent Advances in Germanium Microwave Mixer Diodes *T. Oxley* 239

Equivalent Circuit and Frequency Response Characteristic of the Bandpass Filter comprising Two Coupled Tuned Circuits *R. Bridgen* 249

Design of a High-power u.h.f. Trebler *R. J. Bosselaers* 256

Mullard Technical Communications contains information on the performance or application of Mullard products such as electronic valves and tubes, semiconductor devices, and electrical and magnetic components. It is issued free-of-charge to equipment designers, research organisations, reference libraries, and educational establishments. Bona fide applications to be added to the circulation list should be made under an official letter head to Central Technical Services. Overseas enquiries should be addressed to the local Mullard agent, or to Mullard Overseas Ltd. at Mullard House.

Abstracts, or references to an article, should mention both the source, *Mullard Technical Communications*, and the authors. Requests for republication or translation should be made to the Editor in writing.

The issue of the information contained in this publication does not imply any authority or licence for the utilisation of any patented feature.

'Mullard' is the trade mark of Mullard Limited and is registered in most of the principal countries of the world.

Editor: F. A. Sowan

Assistant Editors: R. Barrie E. G. Evans F. Mills

Published by

Central Technical Services
Mullard Limited, Mullard House, Torrington Place, London, W.C.1
LANgham 6633

© Mullard Limited, 1965

Made and Printed in England by
WIGHTMAN AND COMPANY LIMITED, 1/3 BRIXTON ROAD, LONDON, S.W.9

Effect of Reverse Recovery Time of Thyristors on Efficiency of Parallel Inverters

K. H. WILLIAMSON
Mullard Central Application Laboratory

The efficiency of a thyristor parallel inverter decreases as the frequency of operation is raised. The increased losses are largely due to the commutation time of the thyristors becoming a larger portion of the half-cycle period.

The relationship between the reverse recovery time of the thyristors and the inverter efficiency has been derived, and curves have been drawn showing the variation between them.

INTRODUCTION

It is well known that the efficiency of a static inverter using thyristors decreases as the frequency of operation is increased. The maximum frequency of operation is a compromise with the efficiency of the inverter.

The fall-off in efficiency is attributed to the commutation losses becoming a greater portion of the power in the transformer; therefore the turn-off time of the thyristors has a direct effect on the efficiency. The object of this article is to find the correlation between the turn-off or recovery time of the thyristors and the efficiency of a parallel inverter.

INVERTER CIRCUIT

For the analysis given in this article the basic inverter circuit of Fig. 1 is considered, without feedback diodes and working into a resistive load. The operation of this circuit is well known, but for the sake of continuity a brief description of its working will be given.

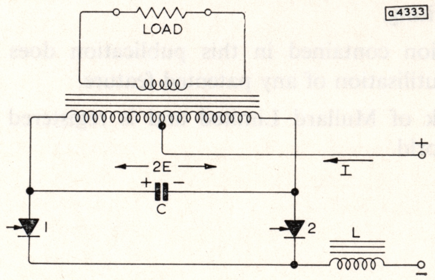

Fig. 1—Inverter circuit

Assume thyristor 2 conducting; then the capacitor C will be charged to a voltage of 2E with the polarity shown, because of transformer action. This gives an output to the load with a polarity depending on the starts and finishes of the transformer windings. Now let thyristor 1 be triggered. The capacitor voltage then appears across thyristor 2 causing it to be reverse biased, and it consequently turns off. During the entire cycle of operation of the inverter the supply current I can be considered constant, because of the series inductance L. Therefore the current is not interrupted but transferred from thyristor 2 to thyristor 1, and it is this transfer period in which we are interested.

We know that the efficiency of an inverter decreases as the commutation period becomes a greater part of the cycle. This is a result of either increasing the frequency of operation of the inverter or of increasing the turn-off or recovery times of the thyristors.

For the efficiency to fall with the output kept constant means that the losses must have increased, because:

$$\text{Efficiency} = \frac{\text{Output}}{\text{Output}+\text{losses}} \times 100\%.$$

It is obvious that all the power loss we observe in practice with decreased efficiency is not dissipated in the thyristors, or the commutating capacitor, and so most of the loss must occur in the transformer and choke as copper losses.

Let us consider the currents in the transformer in greater detail and with reference to the simplified equivalent circuit of Fig. 2 for the period just after the triggering of thyristor 1.

Fig. 2—Equivalent circuit

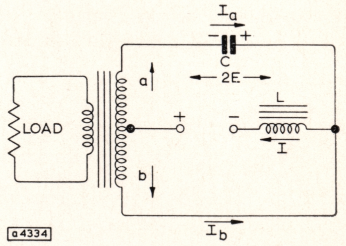

Because of the voltage on the capacitor all the current I will flow through winding 'a' initially; then as C discharges and then charges in the opposite direction, the current in winding 'a' decreases. As I is kept constant, the current in winding 'b' increases such that $I_a + I_b = I$. If we assume linear rise and fall of the currents, which is not unreasonable, the current waveforms during this period are as shown in Fig. 3.

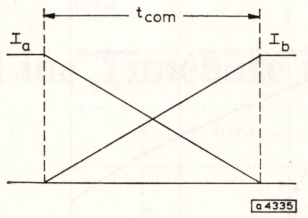

Fig. 3—Current waveforms during commutation

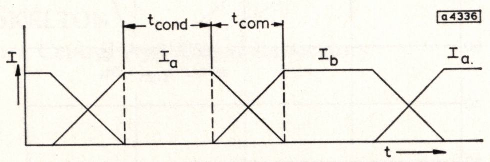

Fig. 4—Current waveforms of transformer primary during conduction and commutation

As these currents are flowing in opposite directions in the transformer the load current is the difference between I_a and I_b, and is zero when $I_a = I_b$. The power output of the transformer is therefore made up of two bits: one the steady output, and the other the output during commutation. The current waveforms in the primary of the transformer are shown in Fig. 4, and the total power output is

$$P_{\mathrm{out}} = I^2R_L(t_{\mathrm{cond}}/\tau)+(I/\sqrt{3})^2R_L(t_{\mathrm{com}}/\tau) \qquad \ldots(1)$$

where t_{cond} = conduction period, t_{com} = commutation period, and $\tau = 1/(2f)$.

Therefore

$$P_{\mathrm{out}} = (I^2R_L/\tau)(t_{\mathrm{cond}}+t_{\mathrm{com}}/3). \qquad \ldots(2)$$

But

$$t_{\mathrm{cond}}+t_{\mathrm{com}} = 1/(2f)$$

where f = frequency of operation; therefore

$$t_{\mathrm{cond}} = 1/(2f)-t_{\mathrm{com}}.$$

Then

$$\begin{aligned} P_{\mathrm{out}} &= (I^2R_L/\tau)[1/(2f)-t_{\mathrm{com}}+(t_{\mathrm{com}}/3)] \\ &= (I^2R_L/\tau)[1/(2f)-\tfrac{2}{3}t_{\mathrm{com}}] \\ &= (I^2R_L/2\tau)(1/f-\tfrac{4}{3}t_{\mathrm{com}}). \qquad \ldots(3) \end{aligned}$$

To maintain the output power at the required value, I^2 must be increased as t_{com} is increased, and the factor by which I^2 must be multiplied to keep P_{out} constant is found as follows. Let the output = 1. Then from Eq.3

$$\begin{aligned} I^2 &= \frac{2}{R_L}\cdot\frac{\tau}{(1/f)-\left(\frac{4}{3}t_{\mathrm{com}}\right)} \\ &= \frac{1}{R_L}\cdot\frac{1}{1-\frac{4}{3}f\,t_{\mathrm{com}}} \qquad \text{since } \tau = 1/(2f). \end{aligned}$$

Therefore

$$I^2 \propto \frac{1}{1-\frac{4}{3}f\,t_{\mathrm{com}}} \propto \text{losses}.$$

DETERMINATION OF VALUE OF t_{com}

In the circuit of Fig. 2, initially $I_a = I$; but when the capacitor voltage reaches zero, $I_a = I_b = I/2$ (ignoring leakage inductance). Therefore the time taken for the capacitor voltage to reach zero is derived as follows:

$$Q = CV = I_{C1}t_{C1}$$

where V = 2E initially, I_{C1} = current through capacitor, and t_{C1} = time for capacitor voltage V_c to fall to zero. When I_{C1} = the mean current between I and I/2, then

$$\frac{I}{2}\left(I+\frac{I}{2}\right) = \frac{3I}{4}$$

therefore

$$\frac{3I}{4}t_{C1} = CV$$

and

$$t_{C1} = \frac{4CV}{3I} = \frac{8}{3}\cdot\frac{CE}{I} = \text{reverse recovery time } t_r.$$

This is the time taken for the capacitor voltage to fall from 2E to zero; so the time taken for the voltage to change from +2E to −2E is derived as follows:

$$Q = CV = I_{C2}t_{C2}$$

where V = 4E, I_{C2} = I/2 because I = 0 when $V_c = -2E$, and t_{C2} = time for V_c to change from +2E to −2E. Therefore

$$\frac{I}{2}t_{C2} = C4E, \text{ and } t_{C2} = \frac{8CE}{I} = \text{commutation time } t_{\mathrm{com}}.$$

However

$$t_{C1} = \frac{8}{3}\cdot\frac{CE}{I} = \text{reverse recovery time } t_r$$

therefore

$$\frac{t_{\mathrm{com}}}{t_r} = \frac{8CE}{I}\cdot\frac{3I}{8CE} = 3$$

and

$$t_{\mathrm{com}} = 3t_r.$$

Hence the current multiplying factor becomes

$$I^2 \propto \frac{1}{1-\frac{4}{3}f\,3t_r} = \frac{1}{1-4f\,t_r}.$$

This is the factor by which I^2 must be multiplied to maintain the output power of the inverter constant for changes in recovery time of the thyristors.

DETERMINATION OF EFFICIENCY

If the commutation time of the thyristors was zero the efficiency would still not be 100%. This is because of the I^2R losses in the transformer and choke plus iron and device losses. A good value of efficiency for a high-frequency inverter without commutation losses would be about 85%. So using this as the basic efficiency, its associated losses are:

$$\text{efficiency} = \frac{\text{output}}{\text{output}+\text{losses}} = 85\%.$$

With output = 1,

$$0{\cdot}85 = \frac{1}{1+\text{losses}}$$

$$\text{therefore losses} = \frac{1-0{\cdot}85}{0{\cdot}85} = 0{\cdot}177.$$

As losses are proportional to I^2, the factor $1/(1\text{-}4f\,t_r)$ can be used to determine the losses and hence the efficiency for any value of t_r up to a limit of $t_{\mathrm{com}} = 1/(2f)$. This is the limiting value beyond which the circuit will become

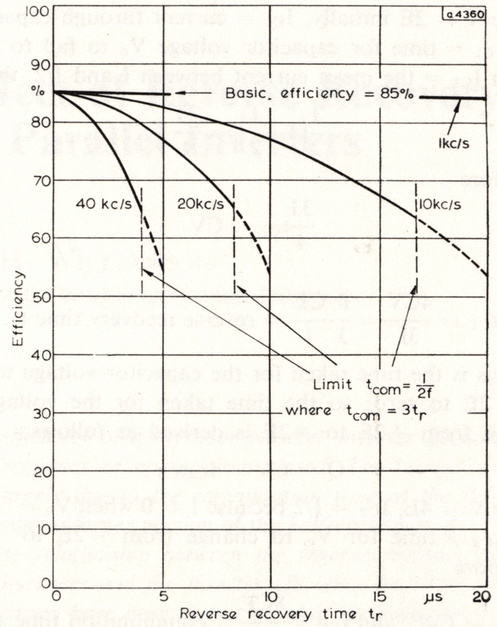

Fig. 5—Efficiency vs reverse recovery time, with basic efficiency of 85%

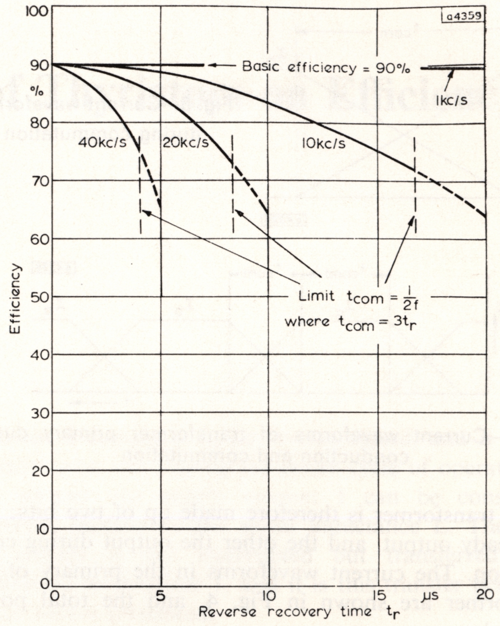

Fig. 6—Efficiency vs reverse recovery time, with basic efficiency of 90%

inoperative owing to the thyristor being triggered before commutation is completed. The efficiency curves are shown in Figs. 5 and 6. They show that there is a fairly rapid drop in efficiency as the recovery time of the thyristors is increased.

With these graphs and the information given it is possible to determine the maximum allowable recovery time for a given frequency of operation and efficiency.

Line Timebase to Scan the A28-13W

D. SKELTON
Mullard Central Application Laboratory

The specification, operating conditions, and performance of a line timebase for the Mullard A28–13W 11in 90° picture tube are given. The timebase operates at 11kV and is switchable for 405 or 625 lines.

INTRODUCTION

The timebase shown in Fig. 1 is intended for operation with the Mullard A28–13W, a 90° narrow-neck 11-inch tube operating at 11kV. It employs a feedback circuit and third-harmonic tuning. The line output transformer is designed to operate on either 405 or 625 lines, it employs a constant flyback ratio of 16%, and switching is provided for:

(i) deflection coil tap
(ii) third-harmonic tuning
(iii) S-correction capacitor
(iv) shaping components.

A saturated inductor is used for the adjustment of linearity.

The timebase is driven by a flywheel sync oscillator incorporating the PCF802 valve.

SPECIFICATION

Deflection Coils

Philips AT1021

Impedance

Line inductance at 1kc/s	1·72mH
Resistance at 20°C	3·46Ω
αH (405 lines)	1·128
αH (625 lines)	1·0785

where αH (the correction factor used for obtaining the volt-amp product VA) $= 1{\cdot}75\frac{R_h . t_h}{L_h}$

R_h being the line coil resistance, L_h the line coil inductance, and t_h the scanning time.

Sensitivity (measured on the A28–13W at 11kV)

Line scan 23·2cm	
Peak-to-peak current	1·47A
VA (405 lines)	2·085
VA (625 lines)	1·995

Saturated Inductor

Philips AT4008T

Fig. 1—Dual-standard stabilised line timebase with switched third-harmonic tuning. All components ±10%, except the 1·5Ω resistor which must be designed so that the DY86 heater voltage is kept within the ±7% limits indicated in Fig. 5

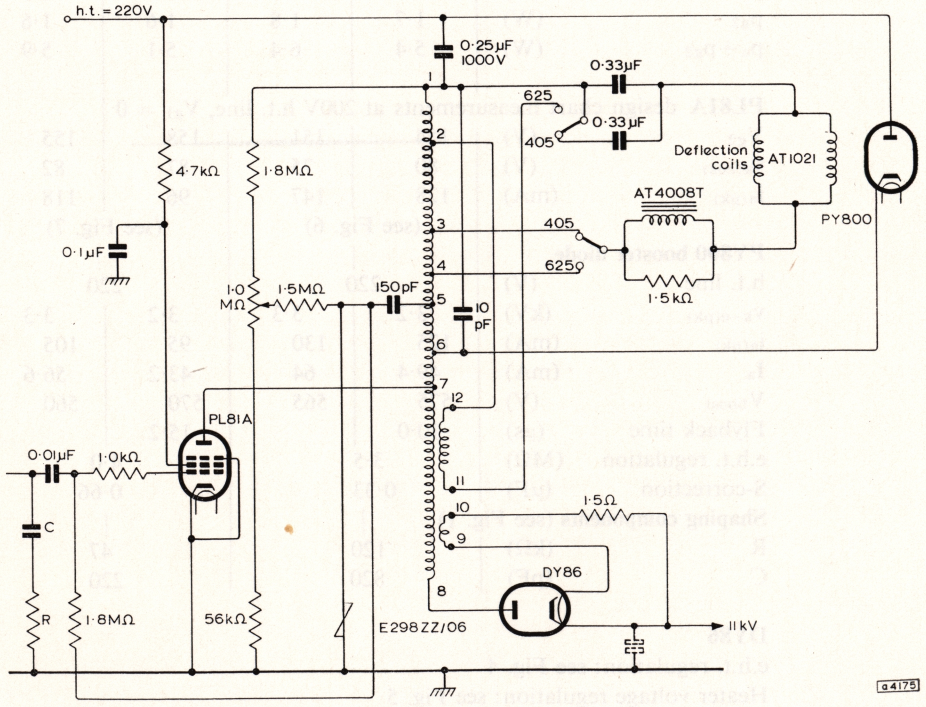

Line Output Transformer

Core	FX2277
Air-gap	0·004in total
Formers (windings 1 to 7 and 7 to 8)	S.R.B.P. with internal diameter 0·435in and wall thickness 0·0625in (two off)
Winding 1 to 7	1130 turns of 32 s.w.g. Bicelflux enamelled copper wire, 60 turns/layer, tapped at 30, 80, 140, 330, and 850 turns, interleaved with two layers of 0·002in paper
Winding 7 to 8	1350 turns of 38 s.w.g. Bicelflux enamelled copper wire, 70 turns/layer, interleaved with 7in length of 0·002in paper
Winding 9 to 10	2 turns of suitably insulated wire
Winding 11 to 12	30 turns of 32 s.w.g. Bicelflux enamelled copper wire on a Perspex bobbin $\frac{5}{8}$in wide
Impregnation	Coils immersed in Okerin 561 at 100°C for 2 hours

MEASUREMENTS

		625 lines		405 lines		Published data limits
Beam current	(μA)	0	200	0	200	
PL81A						
h.t. line	(V)	220		220		
$v_{a(pk)}$	(kV)	4·1	4·2	4·1	4·2	6·0
I_k	(mA)	59	74	52	66	180
I_{g2}	(mA)	9·6	10·3	8·8	9·4	
I_a	(mA)	50	64	43	57	
p_a	(W)	3·7	4·6	3·5	4·3	7·5
p_{g2}	(W)	1·7	1·8	1·6	1·6	4·5
$p_a + p_{g2}$	(W)	5·4	6·4	5·1	5·9	9·5
PL81A design chart measurements at 200V h.t. line, $V_{g1} = 0$						
V_{g2}	(V)	154	151	158	155	
$v_{a(eos)}$	(V)	80	75	87	82	
$i_{a(pk)}$	(mA)	128	147	96	118	
		(see Fig. 6)		(see Fig. 7)		
PY800 booster diode						
h.t. line	(V)	220		220		
$v_{k-e(pk)}$	(kV)	3·2	3·3	3·2	3·3	$v_{h-k} = 5·75$
$i_{a(pk)}$	(mA)	125	130	95	105	350
I_a	(mA)	49·4	64	43·2	56·6	150
V_{boost}	(V)	575	565	570	560	
Flyback time	(μs)	10·0		15·2		
e.h.t. regulation	(MΩ)	3·5		4·0		
S-correction	(μF)	0·33		0·66		
Shaping components (see Fig. 1)						
R	(kΩ)	120		47		
C	(pF)	820		220		

DY86

e.h.t. regulation: see Fig. 4

Heater voltage regulation: see Fig. 5

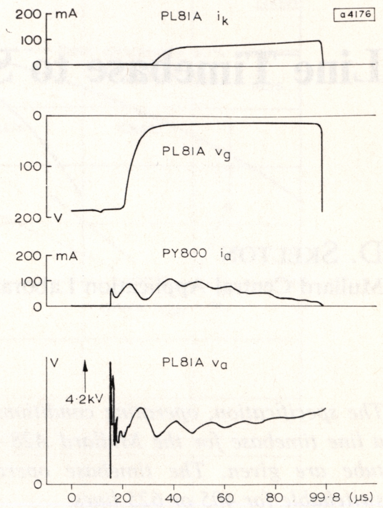

Fig. 2—Waveforms, 405-line operation

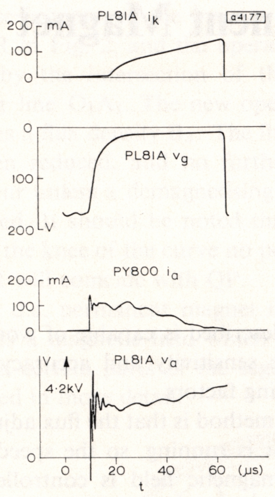

Fig. 3—Waveforms, 625-line operation

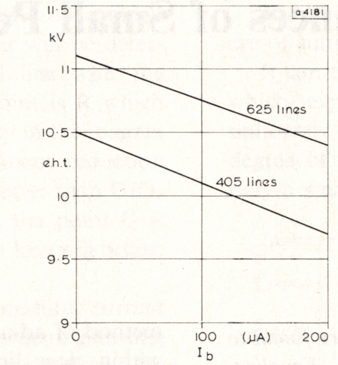

Fig. 4—E.H.T. regulation

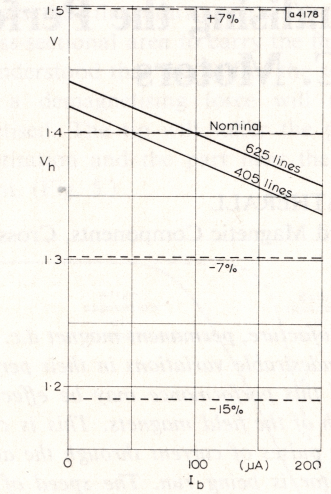

Fig. 5—DY86 heater voltage regulation

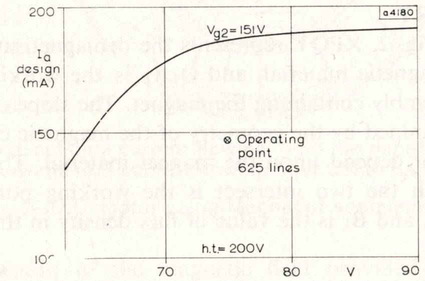

Fig. 6—PL81A stabilised timebase design chart, 625-line operation

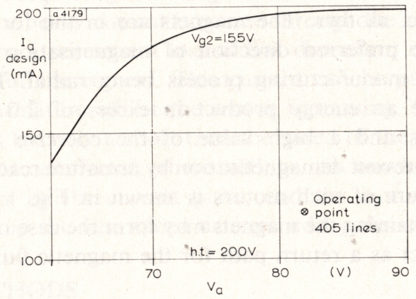

Fig. 7—PL81A stabilised timebase design chart, 405-line operation

Equalising the Performances of Small Permanent Magnet D.C. Motors

J. CATHERALL
Mullard Magnetic Components, Crossens.

In manufacture, permanent magnet d.c. motors are found to have undesirable variations in their performance. Equalisation of this performance may be effected by reducing the strength of the field magnets. This is conveniently done by passing pulses of current through the armature windings as the motor is being run. The speed of the motor may be adjusted to the desired value by the application of a current of the appropriate magnitude. A unit for making such adjustments is described.

INTRODUCTION

Recently developed magnetising techniques have made available ceramic permanent magnets designed specifically for use in d.c. motors. The magnets are in the form of segments, the preferred direction of magnetisation produced in the manufacturing process being radial. These magnets have an energy product in excess of $2{\cdot}0\times10^6$ gauss-oersteds and a high value of the coercive force necessary to prevent demagnetisation by armature reaction.

The structure of such motors is shown in Fig. 1. The steel tube containing the magnets may form the case of the motor, and act as a return path for the magnetic flux.

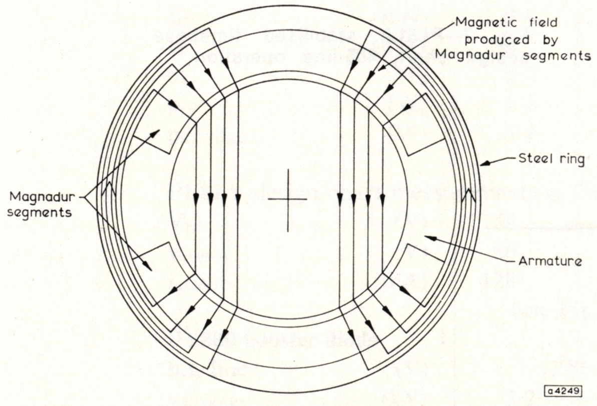

Fig. 1—Motor assembly

The characteristics of the motor, in particular the running speed under no-load conditions, are governed by the number of turns and the resistance of the armature winding, the friction of the bearings and brushes, and the flux produced by the field magnets, the latter normally being the largest variable. It is necessary to control the torque/speed characteristics of the motor within certain limits. This is conveniently done by adjusting the magnetic field to control the no-load speed. The necessary limits will be determined by the application of the motor, while the method of adjustment described is capable of working to within close limits. The sensitivity and accuracy of the tachometer are the limiting factors.

An advantage of this method is that the flux adjustment is made while the motor is running, so the speed of the motor as well as the magnetic field is controlled. The variations in the components of the motor other than the magnet are accounted for.

Since this method of adjustment embraces the partial demagnetisation of the field magnets, it follows that the specification will be determined by the weakest magnets, which may not require adjustment.

THEORY

In Fig. 2, XPQY represents the demagnetisation curve of a magnetic material, and O_1A_1 is the working line of the assembly containing the magnet. The slope of this line is determined by the geometry of the magnetic circuit and does not depend upon the magnet material. The point P at which the two intersect is the working point of the magnet, and B_1 is the value of flux density in the magnet.

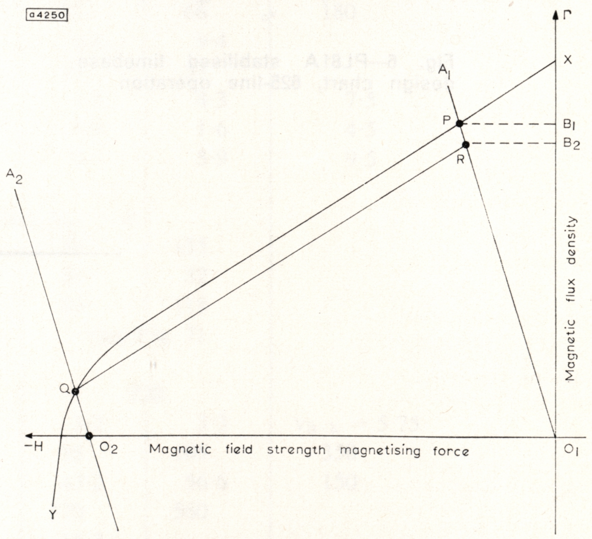

Fig. 2—Demagnetisation curve of magnetic material

If a demagnetising force is now applied to the magnet by a coil wound on the magnet, the working line will be moved to the left by a value O_1O_2 which is determined by the ampere-turns provided by the coil. The slope of the working line is not altered.

The magnet will now be operating at the point on the demagnetisation curve shown at Q. When this demagnetising force is removed the magnet will operate on a recoil line, QR in Fig. 2, and the operating point will be determined by the intersection of this recoil line with the working line O_1A_1. The new operating point is R which produces a flux density B_2. The flux density in the magnet has been reduced, and no further permanent reduction will occur unless a demagnetising force greater than O_1O_2 is applied. It should be noted that unless the point Q is beyond the knee of the curve no permanent loss will occur, and QR will coincide with QP.

In a d.c. permanent magnet motor armature, current produces a magnetic field which acts as a demagnetising force on certain parts of the segments. This will now be examined in more detail.

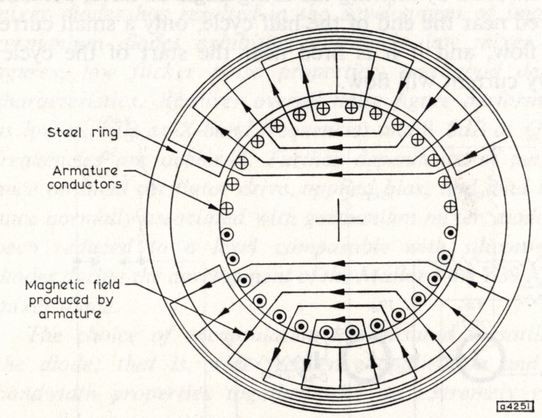

+ Conventional current flowing "into the paper"
● Conventional current flowing "out of the paper"

Fig. 3—D.C. motor using Magnadur segments

The pattern of the magnetic field provided by the armature current is such as to apply a demagnetising force to the left-hand side of the top segment and the right-hand side of the bottom segment. The other halves of the segment experience a magnetising force, which does not have any permanent effect on flux density.

For the parts of the segments that are subject to a demagnetising force it can also be seen that the magnetising force is not uniform around the arc. Close to the centre of the magnet the demagnetising force will be very small as very few ampere-turns are enclosed by this path. When a point further along the arc is considered it can be seen that more ampere-turns are available, and therefore the demagnetising force will be greater. Fig. 4 shows this graphically, and for simplification the segment is shown flat and not arc shaped.

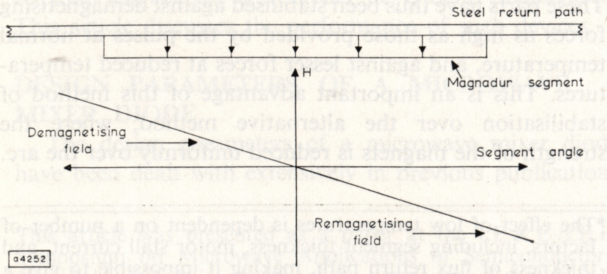

Fig. 4—Effect of demagnetising force on motor segments

The above assumes that the return path and armature are of sufficient cross-sectional area to carry the flux.

It can now be understood that the half of the segment which experiences a demagnetising force will not be uniformly demagnetised. The tip will suffer the greatest degree of demagnetisation and the part near the centre only a small amount. (Fig. 5.)

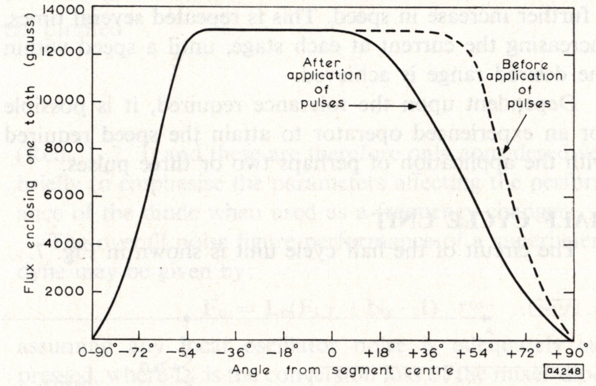

Fig. 5—Non-uniform effect of demagnetisation

If a heavy current is passed through the armature there will be a permanent loss of flux dependent on the magnitude of the current. This current can be passed through the armature whilst the motor is running. If the current flows for only a short time the speed of the motor will be almost unaffected, there will be no overloading of the motor by the current pulse, and the motor will quickly take up the new speed determined by the reduced flux.

METHODS

To provide the necessary current pulses of short duration, a portion of a single half cycle of the 50c/s mains is applied to the motor in series with a fixed resistor of a few ohms. The peak magnitude of the current is determined by the point on the half cycle at which the current is switched on. If this occurs before the point of maximum voltage, the current will achieve the maximum value. If, however, the current is not switched on until after this point, the voltage applied to the motor is less than the maximum and then the current is reduced.

The system is shown diagramatically in Fig. 6. The motor is being driven by a d.c. supply of the correct voltage, and the current pulse is supplied from the half cycle unit. The current pulses are prevented from passing

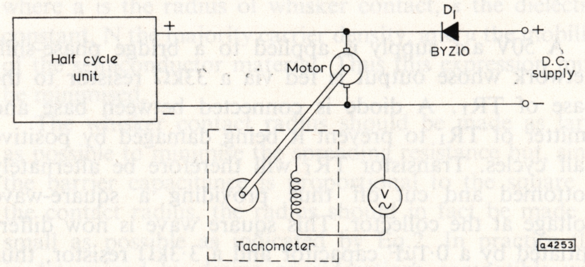

Fig. 6—Pulse source and measurement system

through the d.c. supply by diode D_1. The tachometer generator and voltmeter form a simple method of measuring the speed of the motor.

For normal operation the procedure is as follows. The speed of the fully magnetised motor will be less than the required value. With the phase control set to give a small current a pulse is applied to the motor, and the speed will increase. A heavier current pulse is then applied producing a further increase in speed. This is repeated several times, increasing the current at each stage, until a speed within the desired range is achieved.

Dependent upon the tolerance required, it is possible for an experienced operator to attain the speed required with the application of perhaps two or three pulses.

HALF CYCLE UNIT

The circuit of the half cycle unit is shown in Fig. 7.

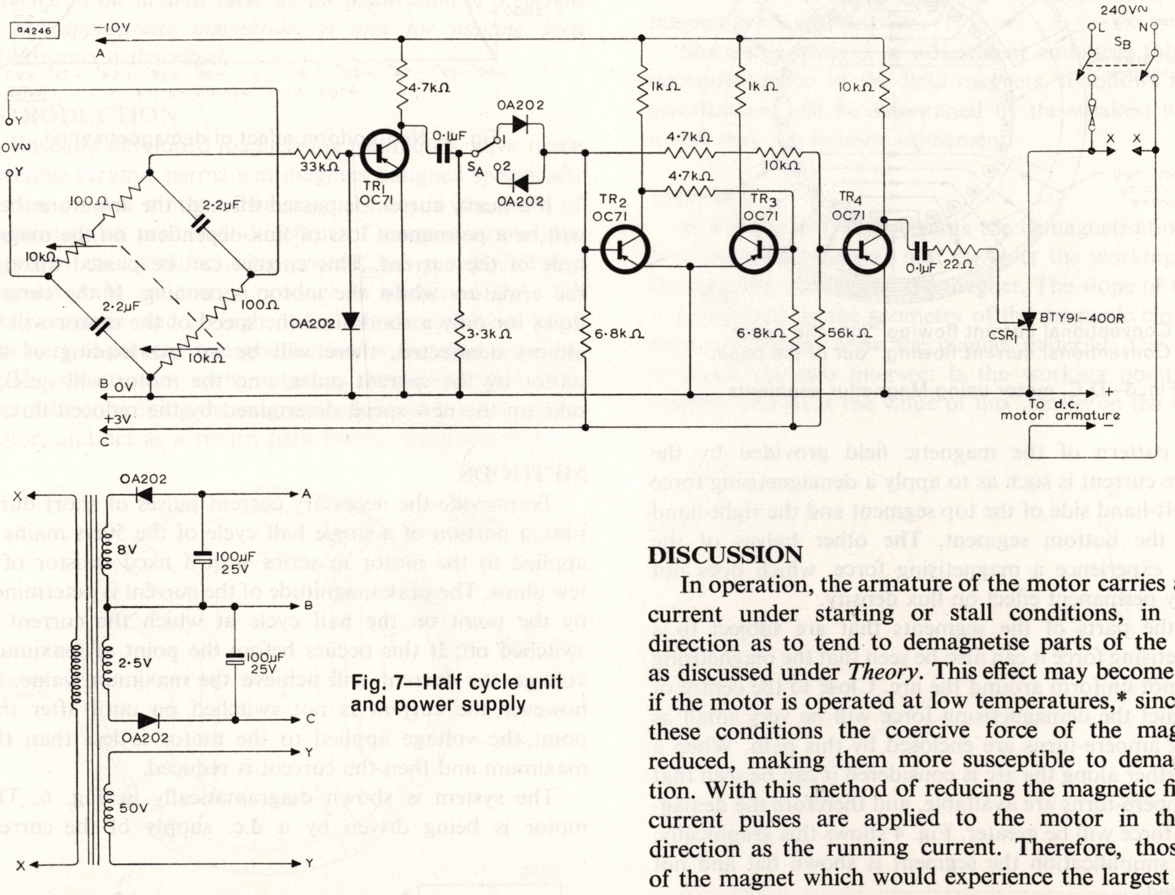

Fig. 7—Half cycle unit and power supply

A 50V a.c. supply is applied to a bridge phase-shift network whose output is fed via a 33kΩ resistor to the base of TR_1. A diode is connected between base and emitter of TR_1 to prevent it being damaged by positive half cycles. Transistor TR_1 will therefore be alternately bottomed and cut off thus providing a square-wave voltage at the collector. This square wave is now differentiated by a 0·1μF capacitor and a 3·3kΩ resistor, thus the input to S_{A1} is a series of alternately positive and negative going spikes, whose phase with respect to a.c. mains can be varied by the 2×10kΩ potentiometer in the phase-shift network.

When S_A is in position 2 the first negative going spike will trigger the bistable circuit comprising TR_2 and TR_3 causing TR_2 to turn on and TR_3 to turn off. The diode OA202 in series with the load to the base of TR_2 prevents the positive spikes resetting the bistable circuit. When TR_3 turns off, TR_4 is turned on, which discharges the 0·1μF capacitor through TR_4, the 22Ω resistor and the CSR_1 gate to cathode path.

Current will flow through CSR_1 and the motor armature for the remainder of the half cycle.

When S_A is returned to position 1 the bistable circuit TR_2, TR_3 is reset to its original state by the first positive going spike applied to the base of TR_2.

The magnitude of current flowing through the armature is controlled by altering the firing angle of CSR_1. If CSR_1 is fired near the end of the half cycle, only a small current will flow, and if it is fired near the start of the cycle a heavy current will flow.

DISCUSSION

In operation, the armature of the motor carries a heavy current under starting or stall conditions, in such a direction as to tend to demagnetise parts of the magnet as discussed under *Theory*. This effect may become serious if the motor is operated at low temperatures,* since under these conditions the coercive force of the magnets is reduced, making them more susceptible to demagnetisation. With this method of reducing the magnetic field, the current pulses are applied to the motor in the same direction as the running current. Therefore, those parts of the magnet which would experience the largest demagnetising force under stall conditions have already experienced a larger demagnetising force from the current pulses. These parts have thus been stabilised against demagnetising forces as high as those provided by the pulses at normal temperature, and against lesser forces at reduced temperatures. This is an important advantage of this method of stabilisation over the alternative method, where the strength of the magnets is reduced uniformly over the arc.

---

*The effect of low temperatures is dependent on a number of factors, including segment thickness, motor stall current, and thickness of flux return path, making it impossible to give a general figure for low temperature limit. A different low temperature limit exists for each design of motor.

Recent Advances in Germanium Microwave Mixer Diodes

T. OXLEY
Wembley Laboratories, Associated Semiconductor Manufacturers Limited

Optimisation of fabrication technology for germanium mixer diodes has resulted in the development of improved germanium diodes exhibiting extremely low mixer noise figures, low flicker noise properties, and good detector characteristics. Receiver overall noise figure performances as low as 6dB at X-band frequencies and 8·5dB at Q-band frequencies are achieved. Further dependence of performance on local oscillator drive, applied bias, and load resistance normally associated with germanium mixer diodes has been reduced to a level comparable with silicon mixer diodes during the development of the Mullard AAY39 X-band mixer diode.

The choice of encapsulation has ensured versatility of the diode; that is, wide frequency application and good bandwidth properties together with an extremely rugged reversible construction.

Experimental evidence suggests a possible further improvement in performance of germanium mixer diodes of about 0·5dB at X-band with greater advantages at higher frequencies.

INTRODUCTION

Silicon was used exclusively during the Second World War and in fact still is used extensively for microwave point-contact rectifiers, applied as frequency changers and detectors. Although the properties of germanium were recognised for this purpose as far back as 1940, because of lack of appropriate technology it was not until about 1955 that a practical device was developed. Germanium mixer diodes, having at least comparable performance with silicon mixer diodes, were described by Messenger and McCoy (Ref. 1) and Lindell and Oxley (Ref. 2). More recently, however, advances in fabrication technology of the germanium microwave point-contact diode have resulted in the development of improved mixer diodes, surpassing the performance of silicon, which achieve typical receiver noise figures as low as 6dB at X-band frequencies and 8·5dB at Q-band frequencies. This article discusses the performance of such devices.

DESIGN PARAMETERS OF A MICROWAVE MIXER DIODE

The design parameters of a microwave mixer diode have been dealt with extensively in previous publications (Refs. 1, 2, 3) and these are therefore only considered very briefly to emphasise the parameters affecting the performance of the diode when used as a frequency changer.

The overall noise figure performance of a superheterodyne may be given by:

$$F_o = L_c(F_{i.f.} + N_r - 1) \qquad \ldots(1)$$

assuming any local oscillator noise is adequately suppressed, where L_c is the conversion loss of the mixer diode, N_r is the noise temperature ratio of the mixer diode, and $F_{i.f.}$ is the noise figure of the i.f. amplifier. Hence, L_c and N_r are the mixer diode parameters determining the value of overall noise figure, and these should be minimised.

A simple diode equivalent circuit is shown in Fig. 1, where C_B represents the barrier capacitance, R_B the barrier resistance and r the spreading resistance. The actual mixing is accomplished by the non-linear barrier resistance; the spreading resistance and barrier capacitance act as parasitics which degrade the conversion loss. The theory of mixing shows that at any frequency at which the barrier capacitance of a mixer diode is important, the product of these parasitics (that is, the spreading resistance and the barrier capacitance) must be minimised for optimum conversion loss and thus satisfactory mixer performance (Refs. 1, 2, 3). It has been shown (Ref. 1) that the value of this product is proportional to:

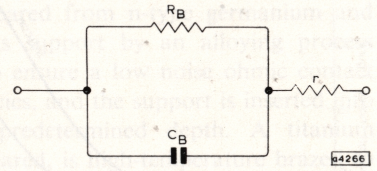

Fig. 1—Simple diode equivalent circuit
Figure of merit of semiconductor material:
$L_C \propto C_B r \propto a\varepsilon^{\frac{1}{2}}/N^{\frac{1}{2}}\mu$

$$a\varepsilon^{\frac{1}{2}}|N^{\frac{1}{2}}\mu \qquad \ldots(2)$$

where a is the radius of whisker contact, ε the dielectric constant, N the majority carrier density, and μ the mobility of the semiconductor material. Thus this expression must be minimised.

The whisker contact radius should be made as large as possible to minimise the spreading resistance but, since the barrier capacitance is proportional to the square of the contact radius, the radius should in fact be made as small as possible as indicated by Eq.2. In practice this is determined by design considerations compatible with satisfactory mechanical stability and resistance to electrical overloads.

In general, though, this expression may be taken as a figure of merit for the semiconductor material, and the

---

This article was presented as a paper at the I.E.R.E./I.E.E. Symposium on Microwave Applications of Semiconductors, June–July 1965. It is reproduced by permission of the I.E.R.E. Programme and Papers Committee.

higher the value of mobility the better the material. There is, however, usually an optimum value for the product of $N^{\frac{1}{2}}\mu$ as the carrier density is increased. For germanium this has been shown (Ref. 1) to occur when the carrier density is about 2×10^{18} carriers/cm^3. The mobility at this concentration is about 800cm^2/Vs. It is of interest to note that this is in good agreement with the resistivity used for the germanium mixer diodes discussed in this article.

Of the other potential semiconductor materials that can be used at normal temperatures (for example, silicon and gallium arsenide) silicon has a mobility less than that of germanium and may thus be expected to be inferior to germanium. However, because of the greater mobility of gallium arsenide and reduced capacitance per unit area normally associated with this material, it may be expected to be a competitor to germanium with a greater cut-off frequency; and so the most significant advantage with the use of gallium arsenide compared with germanium would be at millimetre wavelengths.

The relative merits of these materials may best be demonstrated by examination of mixer performance as a function of frequency. A valuable presentation on this subject has been made by Meredith and Warner (Ref. 4), and Fig. 2 reproduces their theoretical curves of overall noise figure performance as a function of frequency for silicon, germanium, and gallium arsenide. The calculated values assume a constant contact radius, forward d.c. characteristic of the same form, and the same local oscillator voltage amplitude. The greater cut-off frequency, and thus improved mixer performance at millimetre wavelengths, with use of gallium arsenide is clearly indicated. However, in practice the suggested performance has not yet been fully substantiated, possibly because of the lack of experience in point-contact technology with this material. Experimental evidence of gallium arsenide mixer diodes fabricated at the Wembley Laboratories of Associated Semiconductor Manufacturers Ltd., indicated typical overall noise figures in conjunction with a 1·5dB i.f. amplifier of 7·5dB at X-band and 8·8dB at Q-band frequencies.

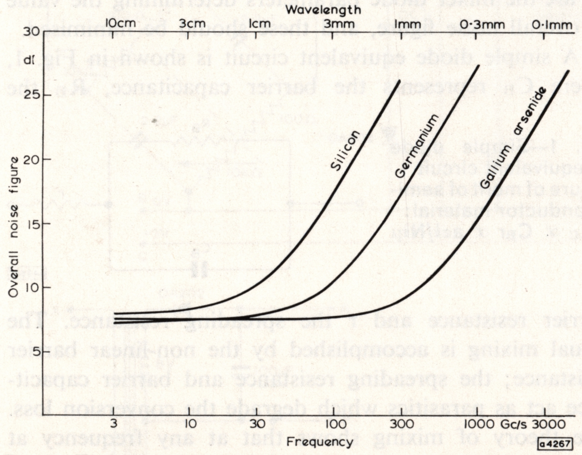

Fig. 2—Theoretical overall noise figure as a function of radio frequency

I.F. noise figure = 1·5 (ratio)
Noise temperature ratio = 1·5

The contact radius assumed for the theoretical estimations shown in Fig. 2 is about $1\cdot25\times10^{-4}$cm, which is fairly typical for diodes designed for millimetre wavelengths. It will be appreciated that for diodes with a larger contact radius, such as those designed for say X-band frequencies, the cut-off frequency will be reduced for each material and the family of curves will be modified towards the lower frequency end of the diagram. The mixer performance shown assumes an i.f. amplifier of 1·8dB and noise temperature ratio of 1·5. Thus for an i.f. amplifier of 1·5dB and noise temperature ratio of 1·0, a theoretical minimum overall noise figure performance of about 5·7dB is suggested for germanium; that is, a diode conversion loss of about 4·2dB when parasitic effects of the barrier capacitance and spreading resistance are completely negligible.

Noise temperature ratio, however, must also be considered for satisfactory mixer performance, as indicated by the equation for overall noise figure. The contributions to noise temperature ratio are the thermal noise of the spreading resistance, shot noise of the barrier, and flicker noise which is characteristic of semiconductors.

It is normally considered that the theoretical concept of minimising conversion loss can be applied to noise temperature ratio as well. This is not so in practice, where experience has shown that noise temperature ratio may be associated with the semiconductor surface treatment, the ohmic back contact, the whisker surface treatment and method of attachment to its support, the method of forming the rectifying contact and, finally, the diode characteristic reverse current leakage.

Theoretical estimates can therefore be made to determine minimum conversion loss for different semiconductor materials and the resistivity requirements for these materials. However, the theory of metal-semiconductor point-contact rectifiers is not yet fully understood and there are many fabrication variables, as already indicated in the previous paragraph, for noise temperature ratio. Such variables have a considerable effect, not only on the noise temperature ratio, but to some extent on conversion loss, and are thus of great importance to the final performance of the device. It is to the optimisation of these fabrication variables that considerable effort has been applied, resulting in the development of improved germanium mixer diodes exhibiting extremely low noise figures.

MIXER DIODE ENCAPSULATION

The physical construction of a mixer diode is largely dictated by the high frequency circuit requirements, and close control of the mechanical tolerances of all component parts is essential, together with control of the dielectric constant of the insulator.

Types of encapsulation in current use are shown in Fig. 3. The cartridge and coaxial types are suitable for use at frequencies up to about 10Gc/s, the plug-in-waveguide for the frequency range 26 to 40Gc/s, and the miniature double-ended capsule for frequencies up to at least 40Gc/s. In fact this type of encapsulation has been used successfully as high as 140Gc/s (Ref. 4).

The X-band cartridge of the 1N23WE type is used extensively by American manufacturers. This is designed primarily for use across X-band waveguide, and its r.f. impedance is fairly high to match the characteristic impedance of the waveguide; whereas the r.f. impedance of the miniature double-ended capsule is relatively low, and thus it is necessary to accommodate a reduced impedance in the design of suitable waveguide mounts. The technique used for test holders has been the design of reduced-height waveguide mounts.

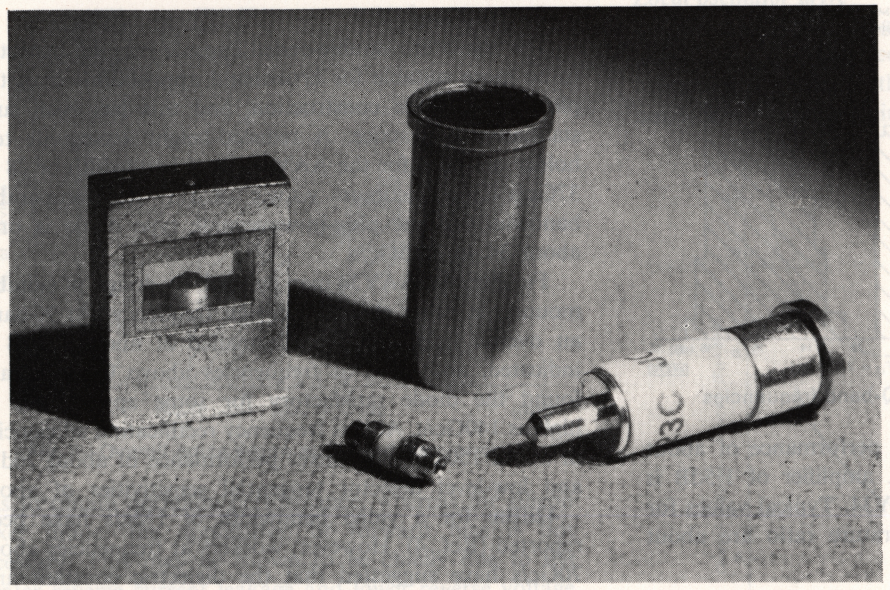

Fig. 3—Types of mixer diode encapsulation

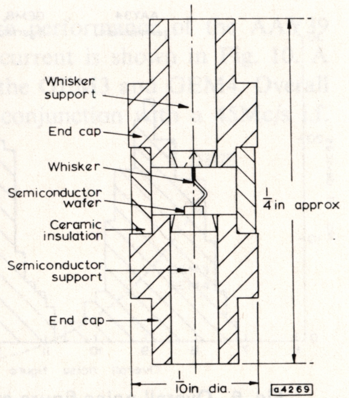

Fig. 5—General arrangement of miniature double-ended capsule

The miniature double-ended capsule was originally developed for use at about 35Gc/s. The construction, however, is extremely versatile. Not only is it suitable for an extremely wide frequency range, but it is also suitable for waveguide, coaxial, and stripline applications and is, of course, reversible.

Further, the small size of the capsule suggests its possible adaptation to standard outlines; thus the design of retrofit units to enable use of the miniature capsule construction in existing equipments. As an example, Fig. 4 illustrates the adaptation of the miniature capsule to the coaxial outline.

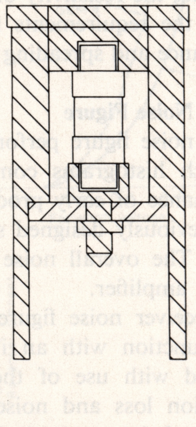

Fig. 4—Adaptation of miniature capsule to coaxial outlines

FABRICATION OF GERMANIUM MIXER DIODES IN THE MINIATURE DOUBLE-ENDED CAPSULE

The miniature double-ended capsule assembly in Fig. 5 shows the method of construction. The end caps are formed from titanium and are bonded to the centre high-alumina ceramic insulating tube by an active-alloy brazing process, to form the metal-ceramic envelope. The whisker and semiconductor wafer supports are made from a low thermal expansion material (to match that of titanium) and are inserted into the envelope. The semiconductor wafer is suitably prepared from n-type germanium and is then bonded to its support by an alloying process specially developed to ensure a low noise ohmic contact at microwave frequencies, and the support is inserted into the envelope to a predetermined depth. A titanium whisker, suitably prepared, is high-temperature brazed to its support and inserted into the envelope to bring the wire into contact with the wafer surface. Both ends of the envelope are sealed by a high-temperature brazing process. The rectifying contact is electro-formed by capacitance discharge techniques to obtain the desired electrical diode characteristics.

The construction thus eliminates entirely the use of epoxy resins or soft solders, resulting in an extremely robust and hermetically sealed reversible capsule, capable of withstanding a wide temperature range.

The electrical performances of such devices, optimised for Q and X-band frequencies, are next described. To facilitate illustration of their performance characteristics, comparison is made freely with current germanium and silicon mixer diode types.

Q-BAND DIODE PERFORMANCE

The Mullard type AAY34 is a germanium mixer diode developed in the miniature capsule outline primarily for use at Q-band frequencies; that is, at 26 to 40Gc/s.

Overall Noise Figure

Noise figure performance is illustrated in Fig. 6, in which histograms compare the overall noise figure performance of early production samples of the AAY34 with previously designed silicon and germanium Q-band diodes. Overall noise figure is related to a 45Mc/s 2dB i.f. amplifier.

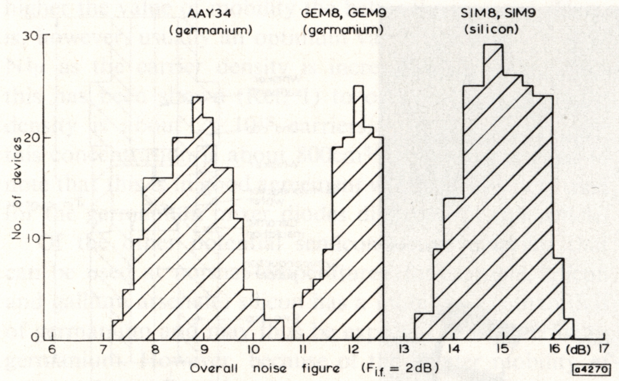

Fig. 6—Overall noise figure at Q-band frequencies

A receiver overall noise figure performance of about 8·5dB in conjunction with an i.f. amplifier of 1·5dB is thus indicated with use of the AAY34. Typical values for conversion loss and noise temperature ratio are about 5·5dB and 1·6 respectively.

Operating Conditions

Optimum noise figure performance for the AAY34 is obtained with a small positive bias, and Fig. 7 illustrates the relationship between overall noise figure, diode rectified current, and applied positive bias voltage. It is clear that optimum noise figure is obtained between 0·1 and 0·2V bias and about 0·5mA total diode current. This relationship is characteristic of the earlier germanium mixer diodes requiring bias to optimise their performance, and is associated with the current-voltage characteristic of the diode (Ref. 2).

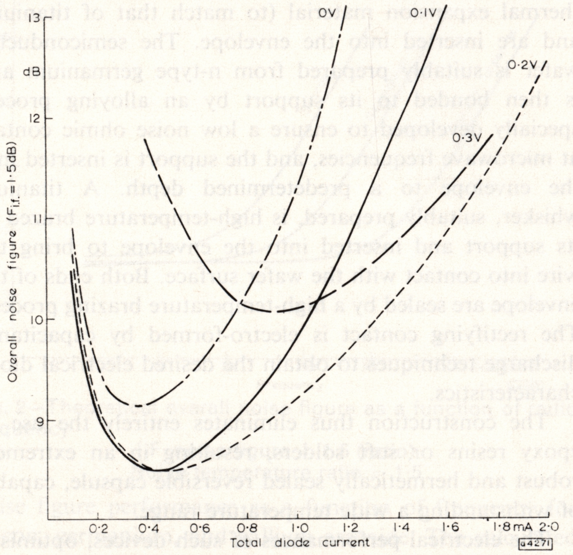

Fig. 7—AAY34: overall noise figure as a function of total diode current, with bias voltage as parameter

I.F. Impedance

Of importance in the design of coupling circuits between the mixer of the i.f. amplifier is the i.f. impedance of the mixer diode; that is, the impedance seen looking into the i.f. terminals of the mixer. The i.f. impedance of the AAY34 at optimum operating conditions is about 700Ω.

Radio Frequency

The miniature double-ended capsule may be expected to be more suitable for broadband applications than the plug-in-waveguide construction, and this has been substantiated in practice. A reduced-height waveguide test holder designed for the AAY34 has a bandwidth of 28 to 37Gc/s for a maximum v.s.w.r. of 2:1. The comparable bandwidth of the plug-in-waveguide type diode is only about 34 to 35·5Gc/s.

Further, the AAY34 may be used, by design of suitable mounts, at other than the design frequency. At X-band an overall noise figure performance of about 7·5dB is indicated, and users at frequencies above Q-band have found the diode satisfactory for some applications as high as 140Gc/s. At this frequency rectification efficiencies of about 150μA/mW, mixer performance of about 20dB, and low-level detector tangential sensitivities of about −42dBm for a video bandwidth of 1Mc/s have been reported (Ref. 4). However, workers at frequencies about 70Gc/s have suggested that the dielectric constant and dimensions of the insulator result in a degradation in performance at this frequency; and, with the same capsule outline dimensions, the use of a different insulator material (such as fused silica) has been found necessary to give satisfactory performance.

X-BAND DIODE PERFORMANCE

The Mullard type AAY39 is a germanium mixer diode developed in the miniature capsule outline primarily for use at X-band frequencies; that is, at about 10Gc/s.

The development of this device followed that of the Q-band diode AAY34; and although the basic fabrication technology incorporated was a direct result of the development of the Q-band diode, further improvement was made feasible by the lower design frequency. For example, a larger junction capacitance could be tolerated, resulting in a lower value of spreading resistance for the same semiconductor material. Thus an improved reverse current-voltage characteristic could be achieved by increasing the resistivity of the semiconductor, still maintaining the requirements for the product of the barrier capacitance and spreading resistance.

Overall Noise Figure

The noise figure performance is illustrated in Fig. 8, in which histograms compare the overall noise figure performance of early production samples of the AAY39 with previously designed silicon and germanium X-band diodes. The overall noise figure is related to a 45Mc/s 2dB i.f. amplifier.

A receiver noise figure performance of about 6·0dB in conjunction with an i.f. amplifier of 1·5dB is thus indicated with use of the AAY39. Typical values for conversion loss and noise temperature ratio are about 4·3dB and 1·1 respectively.

Operating Conditions

It may be worthwhile to examine next how critical the operating conditions are for the AAY39 to achieve this performance, for it will be remembered that mixer diodes incorporating germanium usually require a small positive bias to obtain optimum performance, whereas for silicon mixer diodes the application of forward bias is not necessary. This may be shown to be chiefly due to the greater reverse current leakage and lower reverse voltage breakdown normally associated with a germanium mixer diode compared with those of a silicon type (Ref. 2).

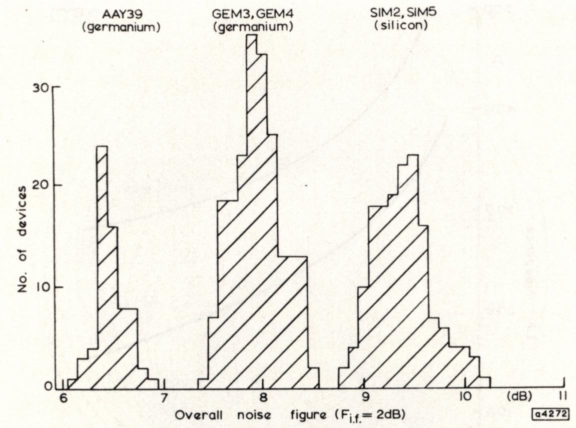

Fig. 8—Overall noise figure at X-band frequencies

The necessity of applying bias to mixer diodes, however, to optimise their performance is quite often regarded as an added design complication for some applications. The germanium types GEM3 and GEM4 were developed as plug-in replacements for the silicon types SIM2 and SIM5 at X-band frequencies to give the improved receiver performance shown in Fig. 8, and were therefore normally operated under zero bias conditions. These conditions are not truly optimum, and the performance of these germanium diodes is therefore fairly dependent on operating conditions, such as local oscillator drive and load resistance. An improved reverse current-voltage characteristic has reduced such effects for operation of the AAY39. The current-voltage characteristics of the AAY39, together with the GEM3 and GEM4, are shown in Fig. 9. This illustrates the reduced reverse current leakage and higher reverse voltage breakdown obtained with the AAY39.

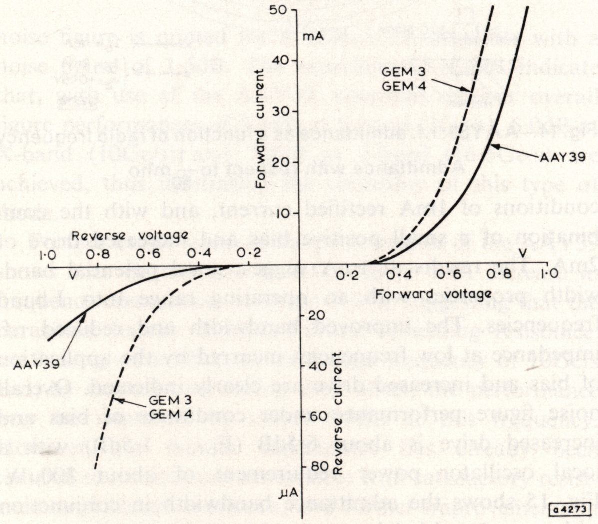

Fig. 9—Current-voltage characteristics

Local oscillator drive

The overall noise figure performance of the AAY39 as a function of rectified current is shown in Fig. 10. A comparison is made with the GEM3 and GEM4. Overall noise figure is quoted in conjunction with a 45Mc/s i.f. amplifier with a noise figure of 2dB. Optimum performance for the AAY39 occurs at about 1mA rectified current, and it can be seen that this performance is fairly independent of rectified current, certainly more so than for the GEM3 and GEM4, and may thus be expected to be fairly independent of local oscillator drive. This is substantiated in Fig. 11, where overall noise figure as a function of local oscillator power is illustrated. Optimum performance is obtained at about 500μW for both the AAY39 and the GEM3 and GEM4; but the superiority of the AAY39 as regards dependence on local oscillator drive, and thus potential increased dynamic range, is clearly indicated. However, a point of interest for applications where local oscillator power is limited is the ability of the AAY39 to operate with reduced local oscillator power provided that a small positive bias is applied to the diode, as shown in Fig. 11. For about 0·15V bias, the optimum local oscillator power may be reduced to about 200μW, and a performance comparable to that of the GEM3 and GEM4 may still be obtained with powers as low as about 50μW.

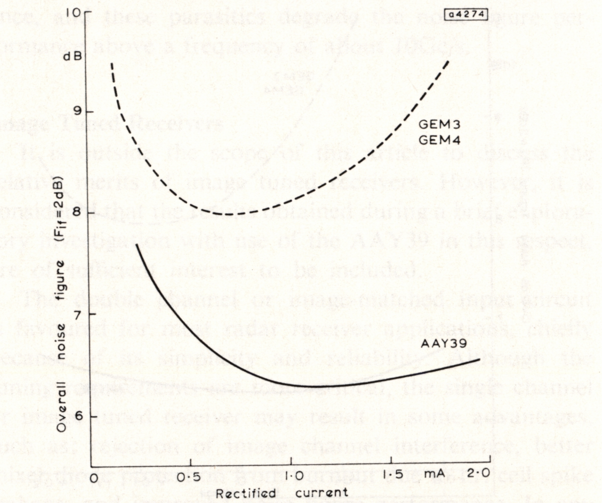

Fig. 10—Overall noise figure as a function of rectified current

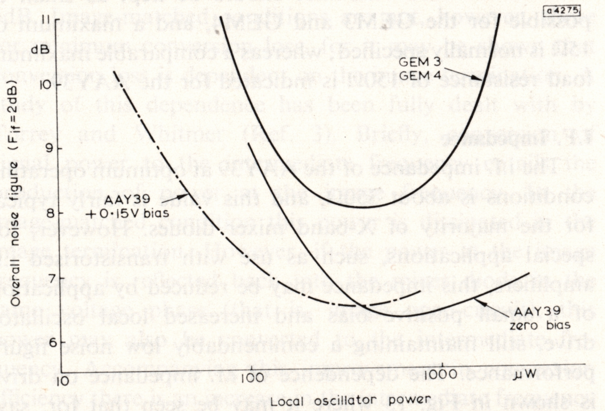

Fig. 11—Overall noise figure as a function of local oscillator power

Bias

The effect of bias on the noise figure performance of the AAY39 and GEM3/GEM4 is shown in Fig. 12. Optimum performance for the AAY39 is not only obtained at zero bias, but is fairly independent of applied bias. As indicated, a large negative bias applied to mixer diodes is always undesirable, the effect being to increase the noise temperature ratio of the diode. A negative bias is developed by the rectified current through the load resistance; this necessitates specifying a maximum load resistance for satisfactory operation of the diode. For a rectified current of 1mA the load resistance should be kept as small as possible for the GEM3 and GEM4, and a maximum of 15Ω is normally specified; whereas a comparable maximum load resistance of 150Ω is indicated for the AAY39.

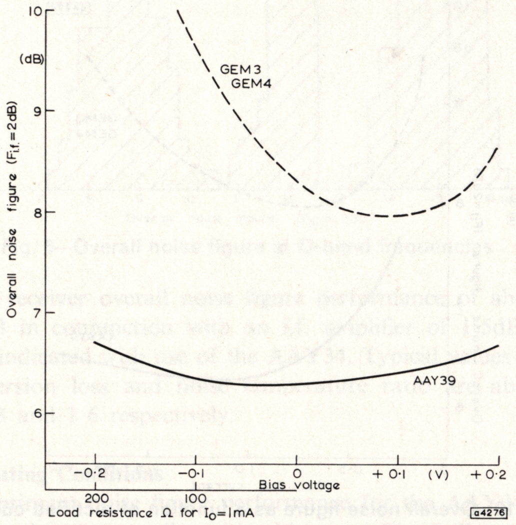

Fig. 12—Overall noise figure as a function of bias voltage

I.F. Impedance

The i.f. impedance of the AAY39 at optimum operating conditions is about 350Ω, and this value is fairly typical for the majority of X-band mixer diodes. However, for special applications, such as use with transistorised i.f. amplifiers, this impedance may be reduced by application of a small positive bias and increased local oscillator drive, still maintaining a commendably low noise figure performance. The dependence of i.f. impedance on drive is shown in Fig. 13 where it may be seen that for, say, 0·15V positive bias and rectified current of 2·0mA, the typical i.f. impedance is about 150Ω. The degradation in noise figure performance from optimum is less than 0·5dB. This aspect may also be of interest where an improved r.f. impedance match for wide bandwidths is required. This is illustrated in the next section.

Radio Frequency

As already indicated, the choice of encapsulation for the AAY39 suggests that the diode can be used at other than its design frequency. Its performance is, therefore, now considered for a wide frequency range.

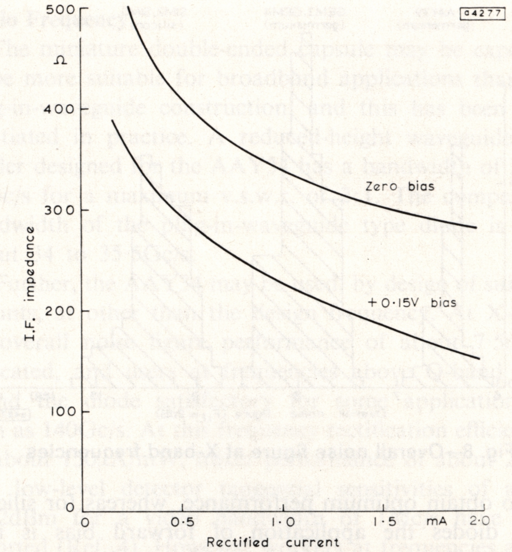

Fig. 13—AAY39: i.f. impedance as a function of diode rectified current

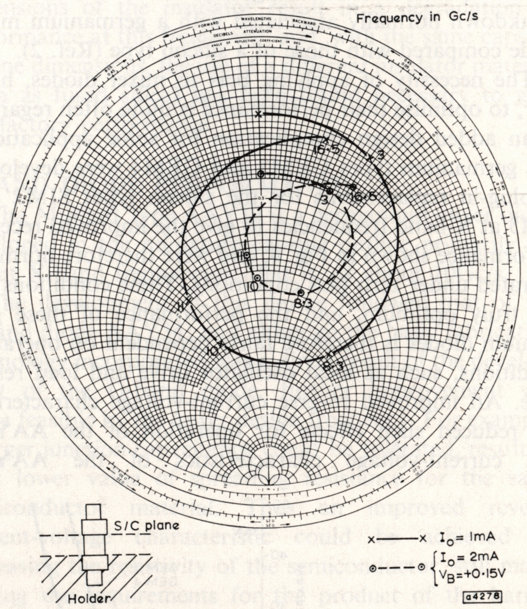

Fig. 14—AAY39: r.f. admittance as a function of radio frequency
Admittance with respect to $\frac{1}{50}$mho

The Smith chart of Fig. 14 shows r.f. admittance, with respect to 1/50mho, of the AAY39 as a function of frequency under two conditions of drive: normal operating conditions of 1mA rectified current, and with the combination of a small positive bias and increased drive of 2mA. The results at 1mA suggest good potential bandwidth properties with an operating range into J-band frequencies. The improved bandwidth and reduced r.f. impedance at low frequencies incurred by the application of bias and increased drive are clearly indicated. Overall noise figure performance under conditions of bias and increased drive is about 6·5dB ($F_{i.f.} = 1·5$dB) with a local oscillator power requirement of about 800μW. Fig. 15 shows the admittance bandwidth in conjunction with a reduced-height waveguide holder designed for X-band frequencies under normal operating conditions. This illustrates a bandwidth of about 8·5 to 10·5Gc/s for a maximum v.s.w.r. of 2:1.

The overall noise figure performance of the AAY39 as a function of frequency is illustrated in Fig. 16. Overall noise figure is quoted for a 45Mc/s i.f. amplifier with a noise figure of 1·5dB. The experimental results indicate that, with use of the AAY39, potential receiver overall figure performances of 5·5dB at S-band (3Gc/s), 6·0dB at X-band (10Gc/s) and 7·0dB at J-band (16·5Gc/s) are achieved, thus illustrating the versatility of this type of diode.

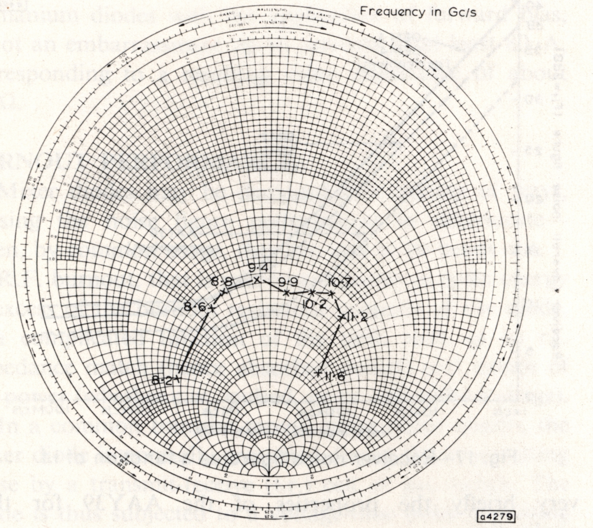

Fig. 15—AAY39: r.f. admittance as a function of radio frequency
Admittance with respect to X-band test holder

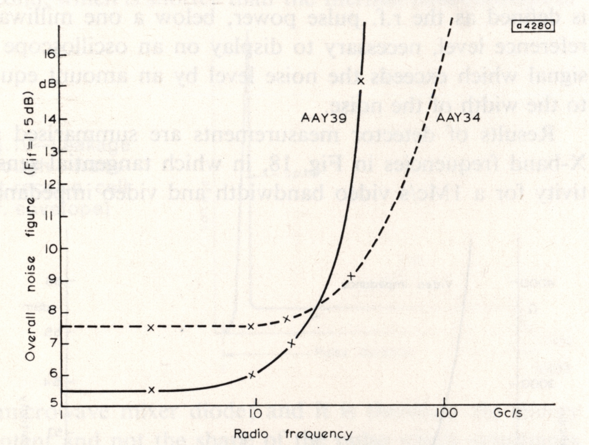

Fig. 16—Overall noise figure as a function of radio frequency

Further examination of the performance of the AAY39 shows that degradation in noise figure with increase in frequency commences at about 3Gc/s, suggesting that the parasitics, barrier capacitance and spreading resistance, are having some effect at the design frequency of 10Gc/s and, by entirely eliminating their effect, the performance may be improved by about 0·5dB at this frequency. However, the barrier capacitance has already been reduced to a minimum compatible with satisfactory resistance to electrical overloads, and further improvements in performance may possibly be best achieved by use of epitaxial techniques. Of further interest is the experimental evidence which indicates a conversion loss of about 4dB at S-band frequencies, which is in fair agreement with the theoretical minimum suggested by Meredith and Warner (Ref. 4).

The Q-band diode AAY34 has been included in Fig. 16 for comparative purposes. This diode exhibits a greater cut-off frequency than the AAY39. This is a result of its higher design frequency and thus reduced value for the product of the spreading resistance and barrier capacitance, and these parasitics degrade the noise figure performance above a frequency of about 10Gc/s.

Image Tuned Receivers

It is outside the scope of this article to discuss the relative merits of image tuned receivers. However, it is considered that the results obtained during a brief exploratory investigation with use of the AAY39 in this respect, are of sufficient interest to be included.

The double channel or image-matched input circuit is favoured for most radar receiver applications, chiefly because of its simplicity and reliability. Although the tuning requirements are more critical, the single channel or image tuned receiver may result in some advantages, such as: rejection of image channel interference, better mixer diode protection from burnout due to t.r. cell spike leakage, and improved noise figure performance. In any case there are receiver requirements for single channel operation, and the possible performance with use of the AAY39 may be of interest.

The noise figure performance of mixer diodes is measured and specified under conditions normally termed the 'broadband case', when the same load admittance is presented to the image and signal channels ('image-matched'). The theoretical minimum limit for the diode conversion loss set by these measurement conditions is 3dB. Image-matched conditions are not, however, those for minimum conversion loss, for it may be shown that conversion loss is dependent on the image termination. A study of this dependence has been fully dealt with by Torrey and Whitmer (Ref. 3). Briefly, conversion of signal power to the intermediate frequency entails the production of power at the image frequency. In the image-matched condition this power is dissipated in the image termination. However, if the power at the image frequency is reflected back into the mixer diode in the same voltage phase (that is, image open-circuit), this power may also be converted to the intermediate frequency. Accompanying this improvement in conversion efficiency there is an increase in the intermediate frequency impedance of the diode and, consequently, an increase in the diode noise temperature ratio.

The results of the investigation into the performance of the AAY39 under image-reflected conditions are shown in Table 1 (p. 246). They may be summarised by reference to the overall noise figure performance, where it may be seen that under conditions for image open-circuit, a receiver noise figure performance at X-band of about 5·0dB could probably be achieved.

Flicker Noise

Recent increase in the use of doppler radars has influenced the interest in mixer diodes for this application. The performance of the AAY39 has therefore been examined.

TABLE 1

Performance of AAY39 under Image-reflected Conditions

Image Termination	I.F. Impedance (Ω)	Noise Temperature Ratio	Conversion Loss (dB)	Overall Noise Figure $F_{i.f.}$ = 1·5dB (dB)
Match	350	1·15	4·2	6·0
Open-circuit	650	1·5	2·2	4·9
Short-circuit	220	1·0	4·7	6·2

As already discussed, the noise figure of any superheterodyne microwave receiver is dependent on the conversion loss and noise temperature ratio of the mixer diode. In general, the conversion loss is independent of the receiver intermediate frequency; but, because of the flicker noise contribution to the noise temperature ratio characteristic, the overall noise figure of the receiver deteriorates as the intermediate frequency is reduced. Pulse radars, where intermediate frequencies of 30 to 60Mc/s are common, are not greatly affected by the flicker noise properties of the mixer diode; but with c.w. doppler radars, the flicker noise properties of the diode are of great importance and can result in serious degradation in receiver sensitivity.

Although the origin of flicker noise in semiconductors is not precisely understood, it is known, as with noise temperature ratio, that the fabrication processes play an important part. Also, the noise is associated with the reverse current leakage of the diode and may be minimised by reducing the reverse current or by limiting the amplitude of the local oscillator voltage (Ref. 5).

To estimate the flicker noise properties of the AAY39, measurements were made of noise temperature ratio at intermediate frequencies in the audio range; and from knowledge of the diode conversion loss, the receiver overall noise figure performance was calculated assuming an i.f. amplifier noise figure of 2dB. Fig. 17 shows this performance at X-band as a function of intermediate frequency, and comparison is made with earlier X-band mixer diodes. The flicker noise properties of germanium mixer diodes are normally expected to be greater than for silicon, as illustrated in Fig. 17. However, the AAY39 not only exhibits better flicker noise properties than the germanium types; but an improvement in performance of doppler systems of about 6dB is indicated by its use, compared with the silicon types.

Low-level Detection

Point-contact diodes have been used for many years as low-level video detectors of radio frequency energy both in microwave receivers and in laboratory measuring equipments. It may therefore be of interest to examine very briefly the properties of the AAY39 for this application.

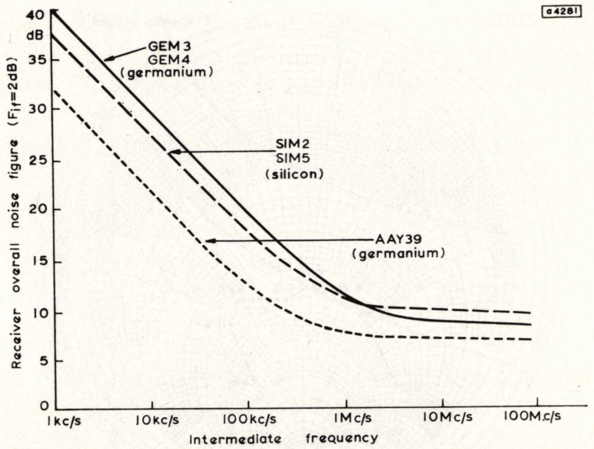

Fig. 17—Receiver noise figure as a function of i.f.

One method of representing the sensitivity of video receivers is by measurement of tangential sensitivity. This is defined as the r.f. pulse power, below a one milliwatt reference level, necessary to display on an oscilloscope a signal which exceeds the noise level by an amount equal to the width of the noise.

Results of detector measurements are summarised at X-band frequencies in Fig. 18, in which tangential sensitivity for a 1Mc/s video bandwidth and video impedance are illustrated as functions of forward bias current. Conventional detector diodes are usually biased in the forward direction, not only for any resulting improvement in their sensitivity but also to take advantage of the associated reduction in video impedance. The lower video impedance in turn provides improved r.f. impedance match over wide bandwidths. The tangential sensitivity of −52dBm indicated for the AAY39 is comparable to the performance of the best conventional detector diode commercially available; further, by the application of forward bias, the video impedance may be reduced to less than 1000Ω. Because of the low noise characteristics of the AAY39, the increase in the magnitude of noise generated within the diode, normally associated with germanium diodes with the application of forward bias, is not an embarrassment up to currents of at least 80μA, corresponding to a resulting video impedance of about 500Ω.

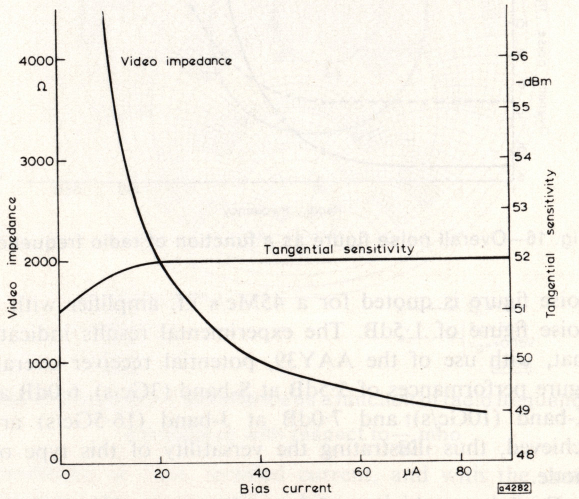

Fig. 18—AAY39: low-level detector performance

BURNOUT PERFORMANCE

Mixer diodes may be damaged in a variety of ways, causing the noise figure performance to deteriorate—when, by common usage, they are said to be burnt out.

R.F. burnout, that is microwave power or spike energy in excess of the burnout resistance property of the diode, is a complicated function of the unit, such as its r.f. impedance match (hence absorbed power) and nature of the power (whether c.w., pulsed, or t.r. cell spike leakage).

In a common transmit-receive pulse radar system, the mixer diode is normally protected during the transmitting pulse by a transmit-receive (t.r.) cell or gas switch. The diode is thus subjected to a voltage-time pulse consisting of a spike followed by a flat response, as shown in Fig. 19. The width of the spike is believed to be about a nanosecond, which is shorter than the thermal time-constant of a microwave mixer diode; and it is therefore the energy content and not the shape of the pulse which determines the temperature attained at the contact and thus the burnout of the diode. There are, however, inherent difficulties in measuring the absorbed power or energy from microwave pulses, which is specially true in the case of a t.r. cell spike. Further, the measured spike energy is usually an average of a number of pulses; but a single spike of abnormal energy may be the sole cause of diode burnout. T.R. cell spike leakage may be simulated by d.c. spikes produced by a co-axial line discharge; and, as the consistency between spikes produced in this manner is believed to be far greater than between t.r. cell leakage spikes, d.c. spike burnout tests are often preferred to assess burnout properties of mixer diodes. Unfortunately, however, a direct correlation between r.f. and d.c. burnout has not yet been established, and there is experimental evidence to show that the d.c. burnout level is dependent on the number of applied spikes. For instance, some mixer diode manufacturers prefer single d.c. spike tests, although in Britain, 5000 spikes are normally specified. Experience has shown that the application of 5000 d.c. spikes has a ten times more drastic effect than a single spike of the same energy. Further, an increase in the number of spikes to about 10^6 will again have a further effect and decrease the apparent burnout level. As an example, Fig. 20 examines the experimental results found for the X-band germanium mixer diodes GEM3 and GEM4. These diodes have a satisfactory r.f. performance, their life exceeding 1000 hours behind a t.r. cell with a spike leakage of 0·2 ergs/pulse. However, as illustrated, the d.c. burnout level is 1·6 ergs for a single spike, 0·16 ergs/spike for multiple tests of 5000 spikes, and 0·1 ergs/spike for 5×10^6 spikes.

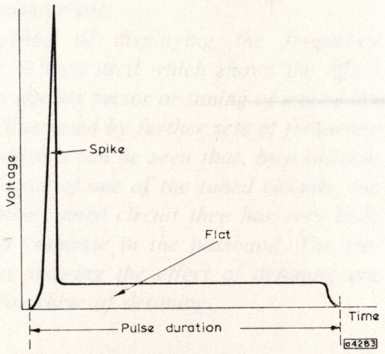

Fig. 19—Leakage through transmit-receive cell (r.f. envelope)

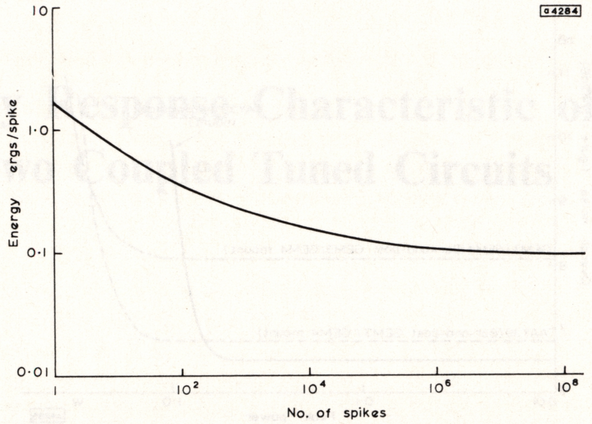

Fig. 20—GEM3, GEM4: burnout as a function of number of d.c. spikes

The burnout properties of the Q-band diode AAY34 have been assessed by multiple d.c. spike and r.f. tests. The experimental evidence indicates a maximum of 0·025 ergs/spike for multiple d.c. tests of 5000 spikes, and r.f. tests demonstrate a satisfactory life performance in balanced mixer circuits in conjunction with t.r. cell type CV2330. The maximum spike leakage specified for this cell is 0·045 ergs/pulse. This performance is comparable with that of current Q-band mixer diodes.

Pulse burnout tests (pulse width about 0·2μs, repetition rate of 2000p/s) carried out on the AAY34 have indicated that 100mW peak is a safe design limit for no deterioration in noise figure performance. The burnout level is about 500mW peak.

For the AAY39, multiple d.c. spike tests of the type normally specified for mixer diodes (5000 spikes) have indicated a burnout level of 0·25 ergs, which compares very favourably with current X-band mixer diodes. Exploratory long-duration d.c. tests, with the application of about 5×10^6 spikes, have indicated a level of about 0·07 ergs.

Extensive t.r. cell leakage tests have not yet been carried out, but initial results in conjunction with current X-band cells demonstrate a performance approaching the level of other X-band mixer diodes.

Results of pulse burnout tests (pulse width 0·5μs, repetition rate 2000p/s) carried out on the AAY39 are shown in Fig. 21 (p. 248) in conjunction with two different types of holder: the waveguide test mount and the coaxial diode bar-and-post type mount. To facilitate tests in conjunction with the coaxial diode mount, the AAY39 was incorporated in an adaptor designed to maintain the coaxial diode outline dimensions and r.f. impedance at X-band frequencies. For comparative purposes, results of tests on the germanium coaxial diode type are included.

The results suggest a safe design limit of 500mW peak power for the AAY39 in conjunction with the waveguide

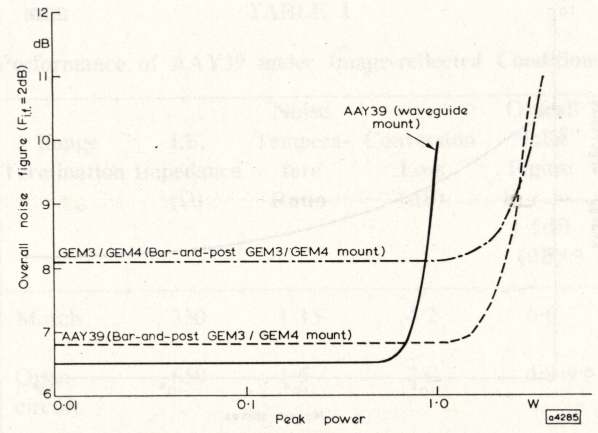

Fig. 21—Pulse burnout: overall noise figure as a function of peak power
Pulse repetition rate = 2000p/s
Pulse duration = 0·5µs

mount, and a comparable safe level with the GEM3 and GEM4 of about 1·5W peak in conjunction with the bar-and-post mount. This emphasises the dependence of burnout behaviour on the diode mount.

REFERENCES

1. MESSENGER, G. C. and MCCOY, C. T. 'A Low Noise-figure, Microwave Crystal Diode'. **I.R.E. Convention Record,** 1955, Part 8, pp. 68 to 73.
2. LINDELL, A. and OXLEY, T. 'Radar Crystal Valves'. **Proc. I.E.E.,** Vol. 106, Part B, Supp. 15, May 1959, pp. 426 to 433.
3. TORREY, H. C. and WHITMER, C. A. 'Crystal Rectifiers'. M.I.T. Radiation Laboratory Series, McGraw-Hill, 1948.
4. MEREDITH, R. and WARNER, F. L. 'Superheterodyne Radiometers for use at 70Gc and 140Gc'. **I.E.E.E. Trans. on Microwave Theory and Techniques,** Vol. MTT – 11, No. 5, Sept. 1963, pp. 397 to 411.
5. SHURMER, H. V. 'A Crystal Mixer for C.W. Radars'. **Proc. I.E.E.,** Vol. 110, No. 1, Jan. 1963, pp. 117 to 122.

Equivalent Circuit and Frequency Response Characteristic of the Bandpass Filter comprising Two Coupled Tuned Circuits

R. BRIDGEN
Mullard Central Application Laboratory

A simple equivalent circuit is derived for the bandpass filter. The frequency response characteristic is then examined first of all in terms of the coupling factor and Q ratio: two families of frequency response curves are given for values of the coupling factor of 1 and 1.5, and in addition formulas are given for the skirt response and other properties of the frequency response characteristic.

An alternative method of displaying the frequency response characteristic is then used which shows the effect directly of changing the quality factor or tuning of one of the tuned circuits. This is illustrated by further sets of frequency response curves from which it can be seen that, by a suitable choice of the quality factor of one of the tuned circuits, the quality factor of the other tuned circuit then has very little effect on the frequency response in the passband. The frequency response curves showing the effect of detuning are shown for one particular value of detuning.

INTRODUCTION

The bandpass filter comprising two coupled tuned circuits is a familiar circuit to both students and engineers engaged in electrical communications.

There are numerous variants of the bandpass filter consisting of two coupled tuned circuits, depending on the type of coupling and on whether the tuned circuits are parallel or series tuned. However, when considering the passband response it is normally not considered necessary to differentiate between the various forms of coupling, provided it is by means of purely reactive elements, or to decide whether the tuned circuits are truly parallel or series tuned, provided the quality factors of the tuned circuits are greater than about 10 (see Appendix 1). We shall accordingly consider the case of mutual inductance coupling, with one of the tuned circuits parallel tuned and the other circuit series tuned, as this case can be easily analysed without making any approximations.

In the first part of this article a simple equivalent circuit of the bandpass filter is derived. This equivalent circuit assists in understanding the physical significance of the parameters used to specify the bandpass filter, and is also used as the basis for the discussion of the frequency response in the following section of the article.

The discussion of the frequency response is divided into two parts. In the first part the basic properties of the frequency response characteristic are briefly described in a fairly conventional manner. In the second part, however, the frequency response is considered in a less usual manner in order to determine the effect of changing the quality factor or tuning of one of the tuned circuits only.

EQUIVALENT CIRCUIT

The circuit which we are considering is shown in Fig. 1, in which the two tuned circuits are assumed to be synchronously tuned; detuning is taken into account later on by simply adding a suitable shunt or series susceptance to one or other of the tuned circuits. As we are dealing with tuned circuits it is convenient to use as the frequency variable:

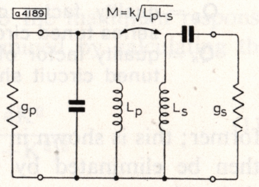

Fig. 1—Inductively coupled bandpass filter with parallel series tuning

$$x = (f/f_o) - (f_o/f), \qquad \ldots(1)$$

where f = frequency

and f_o = the resonant frequency of both tuned circuits.

It will be remembered that the susceptance of a parallel tuned circuit in terms of this frequency variable is given by:

$$b_p = xb_o \qquad \ldots(2)$$

where

b_o = susceptance of the capacitor at the resonant frequency

and the susceptance of a series tuned circuit is given by:

$$b_s = -b_o/x. \qquad \ldots(3)$$

The first stage in simplifying the basic circuit is to replace the inductively coupled inductors by an equivalent circuit in which the coupling is provided by an ideal trans-

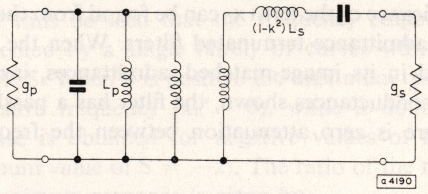

Ideal transformer impedance ratio = $L_p : k^2L_s$
Fig. 2—Equivalent circuit of Fig. 1 with inductively coupled inductors replaced by ideal transformer and non-coupled inductors

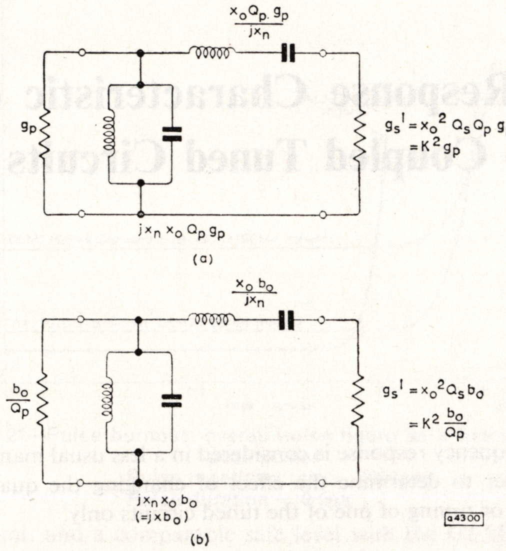
$\frac{x_oQ_p\,g_p}{jx_n}$
g_p
$g_s{}^1 = x_o{}^2 Q_s Q_p g_p = K^2 g_p$
$jx_n x_o Q_p g_p$
(a)
$\frac{x_o b_o}{jx_n}$
$\frac{b_o}{Q_p}$
$g_s{}^1 = x_o{}^2 Q_s b_o = K^2 \frac{b_o}{Q_p}$
$jx_n x_o b_o$ $(=jxb_o)$
(b)
a4300

Fig. 3—Equivalent circuit of Fig. 2 with all components referred across the parallel tuned circuit in terms of (a) the primary conductance g_p and (b) the capacitive susceptance of the parallel tuned circuit b_o

$x_o = k/\sqrt{(1-k^2)}$
$x_n = x/x_o$
$Q_p =$ quality factor of parallel tuned circuit with the series tuned circuit open-circuited
$Q_s =$ quality factor of series tuned circuit with parallel tuned circuit short-circuited

former; this is shown in Fig. 2. The ideal transformer can then be eliminated by transforming all admittances to their values as seen across the parallel tuned circuit, while after some further algebraic manipulation the equivalent circuits shown in Figs. 3a and 3b are obtained. In Fig. 3a all admittances are shown in terms of the primary conductance, while in Fig. 3b all admittances are shown in terms of the capacitor susceptance of the parallel tuned circuit. The universal equivalent circuit of Fig. 4 is obtained by normalising all admittances in terms of the admittance of the parallel tuned circuit at a frequency $x_n = 1$.

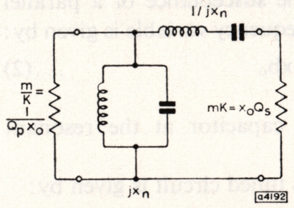

Fig. 4—Universal equivalent circuit in terms of the admittance of the parallel tuned circuit at frequency $x_n = 1$
$m = \sqrt{(Q_s/Q_p)}$
$K = x_o\sqrt{(Q_sQ_p)}$

It will be noticed that the frequency variable has been further modified by putting:

$$x_n = x\bigg/\frac{k}{\sqrt{(1-k^2)}} = \frac{x}{x_o}. \qquad \ldots(4)$$

The significance of the term x_o can be found from the theory of image admittance terminated filters. When the filter is terminated in its image-matched admittances, instead of the fixed conductances shown, the filter has a passband in which there is zero attenuation between the frequencies given by:

$$x = \pm\frac{k}{\sqrt{(1-k^2)}} = \pm x_o. \qquad \ldots(5)$$

This term will consequently be called the bandwidth factor of the filter. In the case of narrow band filters the frequency variable x has a small value in the vicinity of the passband, which allows the following approximation to be used:

$$x \simeq 2\frac{f-f_o}{f_o} \qquad \ldots(6)$$

hence

$$x_n \simeq \frac{f-f_o}{f_p-f_o} \qquad \ldots(7)$$

where

$f_p =$ the frequency at the upper edge of the passband with image matching.

If we now examine the equivalent circuit of Fig. 4 we see that the filter has been reduced to an 'L' section in which the shunt and series arms comprise a parallel and series tuned circuit respectively, while the terminating conductances are specified in terms of the bandwidth factor of the filter x_o and the quality factors of the tuned circuits. For the particular case in which the frequency is the resonant frequency of the tuned circuit the shunt part of the 'L' section becomes open circuit, and the series part short circuit, so that the transformed load conductance x_oQ_s appears directly across the source conductance $1/x_oQ_p$. The ratio of the transformed load conductance to the source conductance is thus

$$\text{Ratio} = x_o{}^2Q_sQ_p = K^2. \qquad \ldots(8)$$

The term K is generally known as the coupling factor.

In the analysis which follows we shall, purely for convenience, consider the parallel tuned circuit as the primary, and the series tuned circuit as being the secondary tuned circuit. It is interesting to note that, provided the quality factor of the secondary circuit is not too low (greater than about 10) and for frequencies not too far away from the resonant frequency of the tuned circuit, the transformed value of the secondary circuit appearing across the primary has the form of a series tuned circuit regardless of whether the secondary circuit is in fact series or parallel tuned.

FREQUENCY RESPONSE

It was noted previously that when the bandpass filter is terminated in its image-matched admittances (which are frequency dependent) it has a passband in which there is zero attenuation between the frequencies given by:

$$x = \pm\frac{k}{\sqrt{(1-k^2)}} = \pm x_o,$$

or

$$x_n = x/x_o = \pm 1. \qquad \ldots(9)$$

The passband width is in fact given approximately by:

$$B \simeq f_ok \quad \text{for } k \ll 1,$$

since

$$B \simeq f_ox_o \text{ and } x_o \simeq k.$$

In the practical case in which the filter is terminated in fixed conductances the frequency response curve is modified to some extent depending on the values of the terminating conductances. The effect of the two terminating conductances on the frequency response can be shown graphically by means of a double family of frequency response curves.

In spite of the fact that there are only two basic variables there are numerous different ways in which these two variables can be combined to provide the two parameter variables for the double family of graphs. We shall now consider two of these choices. The first choice is the normal method of presentation, while the second method is of particular value when it is desired to know the effects of a change of tuning or quality factor of one of the tuned circuits.

Frequency Response Curves using the Coupling Factor (K) and Q Ratio m^2 as Parameters

The transducer loss of the bandpass filter (defined as the ratio of the power in the load to the available power from the source) as a function of the normalised frequency, is readily calculated from the equivalent circuit of Fig. 4, and is given by:

$$L = \frac{4}{x_n{}^2\left(m + \frac{1}{m}\right)^2 + \left(Kx_n{}^2 - K - \frac{1}{K}\right)^2} \qquad \ldots(10)$$

where

$$K = x_o\sqrt{(Q_sQ_p)} \text{ and } m = \sqrt{(Q_s/Q_p)}.$$

A family of frequency response curves plotted from this expression with m as parameter, and K = 1, are shown in Fig. 5, while a second family, with K = 1·5, are shown in Fig. 6. These curves are only drawn for m greater than unity because the same frequency response is obtained for $m = m_K$, and for $m = 1/m_K$, where m_K is a particular value of m.

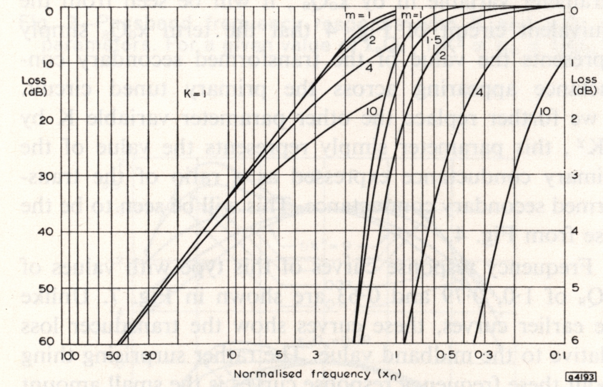

Fig. 5—Transducer loss curves with K = 1·0 and m as parameter

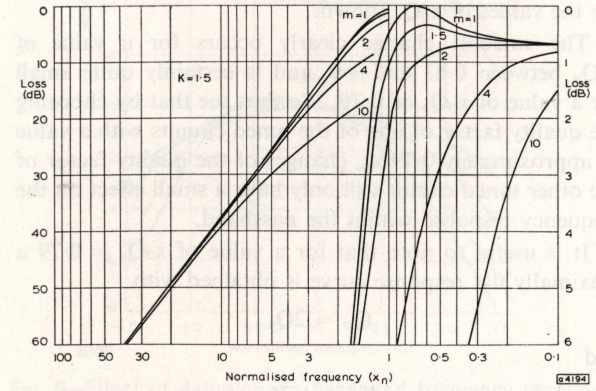

Fig. 6—Transducer loss curves with K = 1·5 and m as parameter

Some of the main characteristics of these frequency response curves will be discussed in the following sections.

Passband width

It will be seen from Figs. 5 and 6 that the edges of the passband still occur approximately at normalised frequencies of plus and minus unity, as for the image terminated bandpass filter, except for extreme values of the Q ratio m^2. The bandwidth factor x_o, which is a function of the coupling coefficient k only, is thus seen to give a useful indication of the bandwidth obtained in practice.

Ratio of the midband to the maximum response

It will be seen from Fig. 6 that for K = 1·5 and m = 1 the response is double humped and passes through zero loss at a value of the normalised frequency x_n approaching unity. This can be shown to be always the case for m = 1, and K greater than unity, the value of the normalised frequency for zero loss becoming closer to unity as K increases.

The ratio of the midband to the maximum response for m = 1, is then easily determined by calculating the midband loss and is given by:

$$L_{(x_n\,=\,0)} = \frac{4K^2}{(1+K^2)^2}. \qquad \ldots(11)$$

Frequency for maximum response

The frequency for maximum response is found by differentiating the frequency response expression and is given by:

$$x_{n(\text{min loss})} = \sqrt{\left[1 - \frac{1}{2K^2}\left(m^2 + \frac{1}{m^2}\right)\right]}. \qquad \ldots(12)$$

Universal frequency response curves

The expression given for the frequency response can be rewritten in the form:

$$L = \frac{L(x_n = 0)}{(x_n')^4 + S(x_n')^2 + 1} \qquad \ldots(13)$$

where

$$S = \frac{m^2 + (1/m^2) - 2K^2}{1+K^2}$$

and

$$x_n' = \frac{x_n}{\sqrt{(1+1/K^2)}}$$

It will thus be seen that the frequency response can be represented by a single family of curves with parameter variable S. When S is positive the maximum response is at the centre frequency $(x_n' = 0)$, while a double-humped response is obtained for negative values of S (up to a maximum value of S = −2). The ratio of the midband to the maximum response is given by:

$$R = 1 - (S^2/4)$$

When S=0 a flat-topped response is obtained which is called the maximally flat response.

Maximally flat response

It has been shown above that the condition for obtaining a maximally flat response curve is given by:

$$S = \frac{m_f^2 + (1/m_f^2) - 2K_f^2}{1 + K_f^2} = 0 \qquad \ldots(14)$$

hence

$$K_f^2 = \tfrac{1}{2}[m_f^2 + (1/m_f^2)] \qquad \ldots(14a)$$

where the subscript f denotes the maximally flat condition. The best known maximally flat response curve is that which is obtained when both the coupling factor K and the Q ratio m^2 are unity (see Fig. 5). It can be seen that the 1dB and 3dB bandwidths of this curve are given by normalised frequencies of $x_n = \pm 1{\cdot}0$ and $x_n = \pm 1{\cdot}41$ respectively. From this starting point maximally flat response curves can be obtained with values of the coupling factor greater than unity by choosing a suitable Q ratio. The ratio between the 3dB and 1dB bandwidths is still 1·41:1, and this fact can be made use of for checking that the response shape is maximally flat. The actual bandwidth, however, in terms of the normalised frequency x_n decreases with increasing coupling factor because of the relationship:

$$x_n = x_n' \sqrt{(1 + 1/K^2)}$$

where x_n' = the normalised frequency variable used for the universal frequency response curves.

In the extreme case of a very large value of the coupling factor the bandwidth decreases by $\sqrt{2}$ times compared with the value for unity coupling factor. The 3dB bandwidth is then given by $x_n = \pm 1{\cdot}0$, while substituting for the required Q ratio gives:

$$K_f/m_f \simeq 0{\cdot}707 \text{ for } K_f \gg 1$$

therefore

$$x_oQ_p \simeq 0{\cdot}707 \text{ for } Q_s > Q_p$$

or

$$x_oQ_s \simeq 0{\cdot}707 \text{ for } Q_p > Q_s.$$

Hence to obtain the same bandwidth as was obtained with a coupling factor of unity and equal quality factors, the bandwidth factor x_0 must be increased by $\sqrt{2}$ times, and the quality factor of one of the tuned circuits must be halved. The quality factor of the other tuned circuit will have a high value which will depend on the actual value of the coupling factor.

Approximate expression for the skirt response

The approximate expression:

$$L_s \simeq \frac{(1 + 1/K^2)^2}{x_n^4} \qquad \ldots(15)$$

holds reasonably well provided:

$$x_n > 2\frac{m}{K},\ x_n > \frac{2}{mK},\ \text{and } x_n > 2,$$

where

$$L_s = \text{loss relative to the midband loss.}$$

It is interesting to note that while the skirt response depends strongly on the bandwidth factor of the filter, x_o, it hardly depends at all upon the Q ratio m^2 and only to a small extent on the coupling factor K.

When considering a bandpass filter in which the two tuned circuits are truly both parallel tuned the above expression should be modified to:

$$L_{s(pp)} \simeq \left(\frac{f}{f_o}\right)^2 \frac{(1 + 1/K^2)^2}{x_n^4} \qquad \ldots(16a)$$

for an inductively coupled filter, and

$$L_{s(pp)} \simeq \left(\frac{f_o}{f}\right)^2 \frac{(1 + 1/K^2)^2}{x_n^4}. \qquad \ldots(16b)$$

for a capacitively coupled filter (see Appendix 3).

Frequency Response Curves using the Coupling Factor K and Factor x_oQ_s as Parameters

The method of presenting the frequency response characteristic described above is not very suitable when it is desired to know the effect of a change of admittance across the parallel tuned circuit or in series with the series tuned circuit. For example, if one considers a gain controlled transistor followed by a bandpass filter, the change in output conductance of the transistor which occurs as the gain is varied may cause a considerable change in quality factor of the primary tuned circuit of the bandpass filter. The effect cannot be easily investigated using frequency response curves of the type which have been considered, because the change of quality factor causes both the coupling factor K and the Q ratio m^2 to vary.

The problem is easily overcome by replacing the parameter variable m by x_oQ_s; it will be seen from the equivalent circuit of Fig. 4 that the term x_oQ_s simply represents the value of the transformed secondary conductance appearing across the primary tuned circuit. If we further replace the other parameter variable K by $1/K^2$, this parameter simply represents the value of the primary conductance expressed as a ratio of the transformed secondary conductance. This will be seen to be the case from Fig. 4.

Frequency response curves of this type with values of x_oQ_s of 1·0, 0·79 and 0·63 are shown in Fig. 7. Unlike the earlier curves, these curves show the transducer loss relative to the midband value. The rather surprising thing about these frequency response curves is the small amount by which the response changes within the passband over the whole range of coupling factors from zero to infinity, for the values of x_oQ_s shown.

The smallest change clearly occurs for a value of x_oQ_s between 0·63 and 1·0, and is certainly quite small for a value of x_oQ_s of 0·79. We thus see that by choosing the quality factor of one of the tuned circuits with a value of approximately $0{\cdot}79/x_o$, changes of the quality factor of the other tuned circuit will only have a small effect on the frequency response within the passband.

It is useful to note that for a value of $x_oQ_s = 0{\cdot}79$ a maximally flat response curve is obtained with:

$$Q_p = 2Q_s$$

and

$$K^2 = 1{\cdot}26.$$

Further, the normalised frequency for the 3dB bandwidth is given by:

$$x_n = \pm 1{\cdot}34.$$

The same type of frequency response curves can also be used to investigate the effect of detuning one of the tuned circuits. In this case the frequency response is simply calculated using the equivalent circuit of Fig. 3a or 3b with a particular value of susceptance across the parallel tuned circuit. The response was calculated directly for the equivalent circuit by means of a digital computer. Families of response curves calculated in this way for a particular value of detuning susceptance are shown in Figs. 8, 9, and 10. These three sets of curves differ from

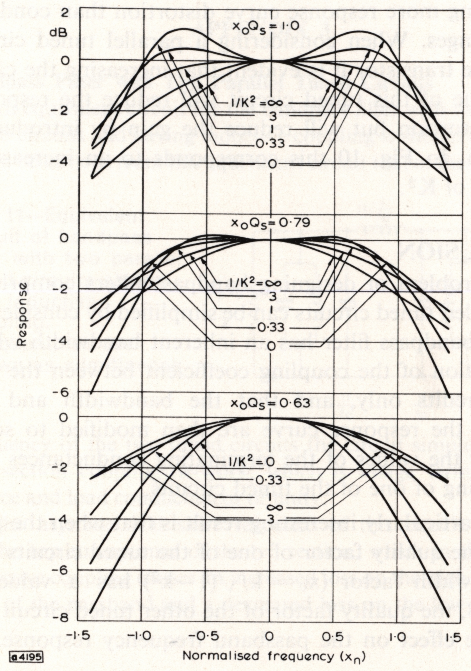

Fig. 7—Passband frequency response with K and x_oQ_s as parameters. For a given value of x_oQ_s, $1/K^2 \propto g_p \propto 1/Q_p$

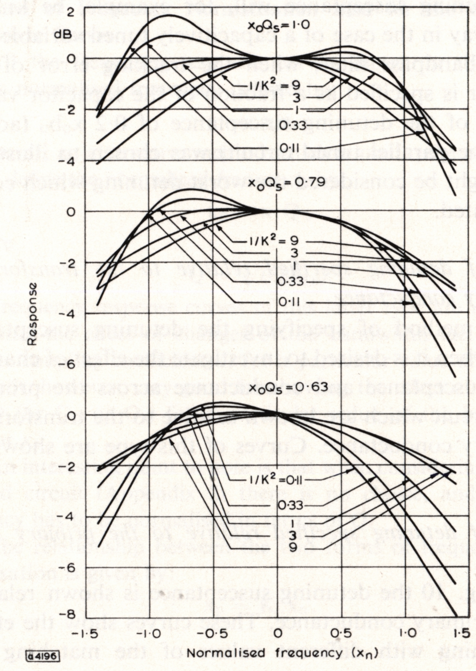

Fig. 8—Effect of detuning on passband frequency response of bandpass filter, with $B = 0{\cdot}2x_ob_o$. For a given value of x_oQ_s, $1/K^2 \propto g_p \propto 1/Q_p$

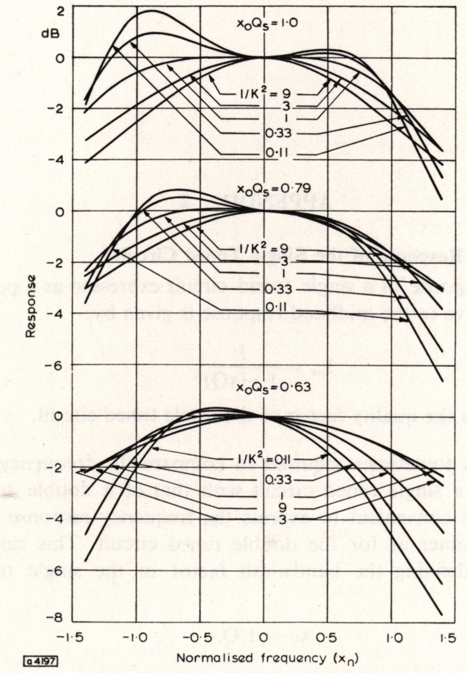

Fig. 9—Effect of detuning on passband frequency response of bandpass filter, with $B = 0{\cdot}25g_s'$. For a given value of x_oQ_s, $1/K^2 \propto g_p \propto 1/Q_p$

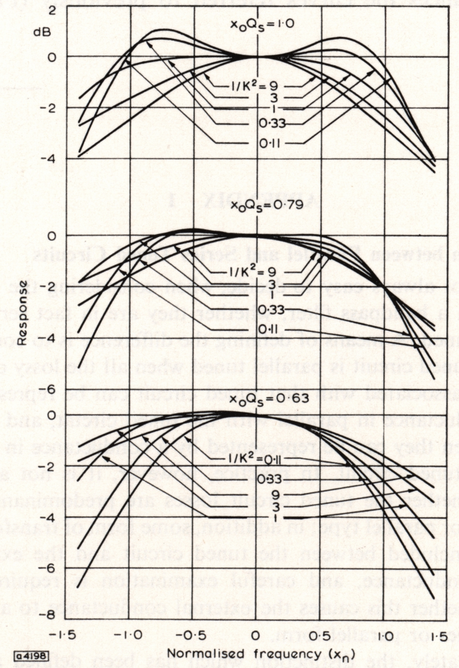

Fig. 10—Effect of detuning on passband frequency response of bandpass filter, with $B = 0{\cdot}4g_p$. For a given value of x_oQ_s, $1/K^2 \propto g_p \propto 1/Q_p$

one another in the way in which the detuning susceptance has been specified: the reason for these differences will be discussed in the following subsections.

Effect of detuning specified relative to the tuned circuit

Fig. 8 shows the effect of detuning one of the tuned circuits by a certain fraction of the capacitor susceptance. The detuning susceptance will, for example, be known in this way in the case of a capacitively tuned variable frequency bandpass filter, when the tracking error of the capacitor is specified as a fraction of the capacitor value. A value of the detuning susceptance of $0{\cdot}2\ x_o b_o$ (added across the parallel tuned circuit) was chosen to illustrate what might be considered the worst detuning which could be tolerated.

Effect of detuning specified relative to the transformed secondary conductance

This method of specifying the detuning susceptance is used when it is desired to investigate the effect of changes of the susceptance and conductance across the primary tuned circuit which are known relative to the transformed secondary conductance. Curves of this type are shown in Fig. 9.

Effect of detuning specified relative to the primary conductance

In Fig. 10 the detuning susceptance is shown relative to the primary conductance. These curves show the effect of detuning with different values of the matching K^2 between the primary and transformed secondary conductances. This variation of matching might occur, for example, in a variable frequency bandpass filter because of the change of susceptance with frequency of the inductor and capacitor comprising the primary tuned circuit. In these circumstances the curves referred to previously (Fig. 8) would not give a clear picture of the effect of the detuning, as different values of matching would cause different values of the detuning susceptance to appear across the primary tuned circuit.

The curves of Fig. 10 are also useful when considering a bandpass filter connected to a gain-controlled transistor in the case when susceptance changes of the transistor are causing more response curve distortion than conductance changes. When considering a parallel tuned circuit across the transistor it is evident that increasing the capacitor value of this tuned circuit will reduce the response curve distortion but will reduce the gain by introducing mismatch. In Fig. 10 this corresponds to an increase in the value of K^2.

CONCLUSION

The problem of designing bandpass filters comprising two coupled tuned circuits can be simplified by considering that the bandpass filter has an inherent bandwidth which is a function of the coupling coefficient between the two tuned circuits only, and that the bandwidth and the shape of the response curve are then modified to some extent by the values of the terminating conductances and by detuning of one of the tuned circuits.

One particularly interesting result is that when the product of the quality factor of one of the tuned circuits and the bandwidth factor ($x_o = k/\sqrt{(1-k^2)}$) has a value of about 0·8, the quality factor of the other tuned circuit has very little effect on the passband frequency response.

ACKNOWLEDGEMENT

The author is indebted to F. C. Clifford for introducing him to the parallel series tuned bandpass filter and for pointing out the advantages of image-matched analysis.

APPENDIX 1

Distinction between Parallel and Series Tuned Circuits

It is not always easy to decide, when considering the tuned circuits in a bandpass filter, whether they are in fact series or parallel tuned. A means of defining the difference is to consider that the tuned circuit is parallel tuned when all the lossy circuit elements associated with that tuned circuit can be represented by a conductance in parallel with the tuned circuit, and series tuned when they can be represented by a conductance in series with the tuned circuit. In practice, however, it is not always known whether the tuned circuit losses are predominantly of the series or parallel type; in addition, some form of transformer is often included between the tuned circuit and the external circuit conductance, and careful examination is required to decide whether this causes the external conductance to appear in the series or parallel form.

Fortunately, the distinction which has been defined above becomes unimportant for frequencies near the resonant frequency, if the quality factor of the tuned circuit is greater than about 10.

APPENDIX 2

Frequency Response of the Single Tuned Circuit

The response of a single tuned circuit expressed as a power ratio relative to the midband response is given by:

$$L_s = \frac{1}{1+(xQ)^2}$$

where Q is the quality factor of the single tuned circuit.

As it is sometimes required to compare the frequency response of a single tuned circuit with that of a double tuned circuit it is convenient to express the frequency response in a similar manner as for the double tuned circuit. This can be done by defining the bandwidth factor of the single tuned circuit by:

$$x_o = 1/Q.$$

The passband frequency response of a single tuned circuit is shown in Fig. 7 by the curve for $x_oQ_s = 1$ and $1/K^2 = \infty$. This curve represents the frequency response of the secondary tuned circuit only, as there is infinite damping across the primary tuned circuit. An approximate expression for the skirt relative to the midband response is given by:

$$L_{s(s)} = \frac{1}{{x_n}^2},$$

and holds reasonably well provided that $x_n > 2$.

APPENDIX 3

Bandpass Filter with Two Parallel Tuned Circuits

An equivalent circuit for the bandpass filter with two parallel tuned circuits and having inductive coupling is shown in Fig. 11. It will be noticed from this equivalent circuit that at the resonance frequency of the two tuned circuits the circuit simplifies into a 'π' section coupling network, which is image terminated by source and load conductances of unity.

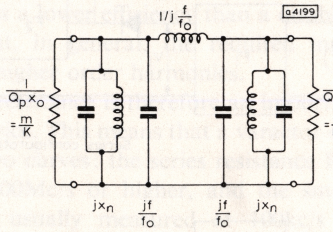
$1/j\frac{f}{f_o}$
a4199
$\frac{1}{Q_p x_o} = \frac{m}{K}$
$\frac{1}{Q_s x_o} = \frac{1}{mK}$
jx_n
$\frac{jf}{f_o}$
$\frac{jf}{f_o}$
jx_n

Fig. 11—Equivalent circuit of bandpass filter with two parallel tuned circuits shown with inductive coupling. All quantities are shown as admittances

The asymmetrical skirt response of this circuit is caused by the top susceptance of the 'π' section, which in the case of inductive coupling causes an increased loss on the high frequency side of the passband and a decreased loss on the low frequency side, compared with the bandpass filter comprising one parallel and one series tuned circuit, which has a symmetrical skirt response.

APPENDIX 4

Method of Frequency Normalisation used for the Frequency Response Curves

All the frequency response curves shown in this article use a normalised frequency defined by:

$$x_n = x/x_o.$$

However, an alternative method which is used quite commonly is to define the normalised frequency by:

$$x_p = x.Q,$$

where

$$Q = \sqrt{(Q_sQ_p)}.$$

Frequency response curves of this latter type are useful for showing the effect of changes of the bandwidth factor x_o (or of the coupling coefficient k) for a particular value of Q. They are not, however, very good for showing the effect of a change of Q (or Q_p or Q_s) for a particular value of the bandwidth factor x_o.

An interesting point to note is that when considering a single tuned circuit (Appendix 2) there is no choice, and the frequency has to be normalised in terms of Q.

The relationship between the two forms of frequency normalisation is given by:

$$x_p = K.x_n.$$

Design of a High-power u.h.f. Trebler

R. J. Bosselaers
Amperex Electronic Corporation, Cranston, R.I., U.S.A.

Considerable extension of the power and frequency capabilities of solid-state transmitters has been made possible by recent developments in semiconductor technology. This article discusses the design of varactor trebler circuits that operate at 75% efficiency in the 150 to 450Mc/s region at input powers of about 30W. A practical circuit, using the BAY96 varactor diode, is given.

INTRODUCTION

High power at high frequencies is still the domain of vacuum tube devices. However, the rapid expansion of solid state device technology in recent years has made available transistors that can produce 50W at 50Mc/s or 15W at 175Mc/s. These power levels can be doubled or trebled by parallel connection of several units. At the same time efficient, high-power varactors have been developed which enable an expansion of the frequency range by a factor of three or more.

The concept of harmonic generation with non-linear reactances is not new; but only in recent years, due to the silicon planar technology, has it been possible to manufacture suitable devices with a high-yield low-cost process and reproducible characteristics. Efficiencies of 75% are now possible in the 150 to 450Mc/s region at input power levels of 30W. Therefore, the design of completely solid-state transmitters with a 24W output at 470Mc/s is now possible. This article deals with the basic concepts of harmonic generation and provides practical guide lines for the design of varactor trebler circuits.

ELEMENTARY CONCEPTS

The varactor diode can be interpreted as a nonlinear capacitance, whose functional dependence on voltage is:

$$C = K(V+\phi)^{-\gamma} \qquad \ldots(1)$$

where C is the small-signal capacitance, V is the reverse voltage applied across the junction, and ϕ is the contact potential which is characteristic of the semiconductor material. The value γ depends on the impurity diffusion profile. The theoretical value of γ is 0·5 for an abrupt junction and 0·33 for a graded junction. Commercial diodes usually have a γ value between that of an abrupt and graded profile.

The small-signal capacitance can be defined as:

$$C = dQ/dV \qquad \ldots(2)$$

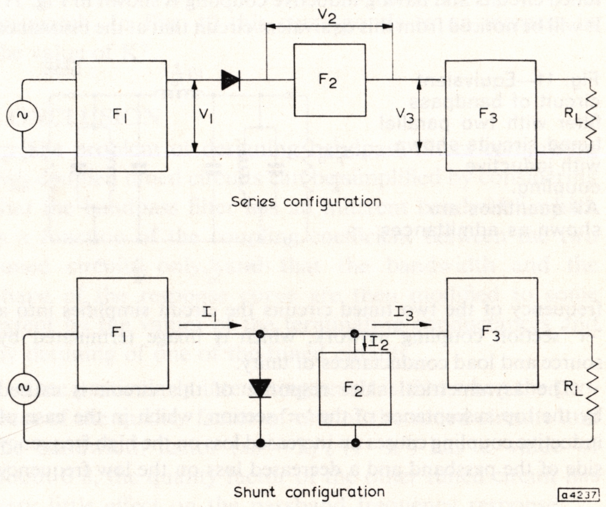

Fig. 1—Two possible circuit approaches

where Q is the charge. Combining Eqs.1 and 2 we obtain:

$$dQ/dV = K(V+\phi)^{-\gamma}$$

$$Q = \int K(V+\phi)^{-\gamma}dV = \frac{K[(V+\phi)^{1-\gamma}]}{1-\gamma}.$$

therefore

$$Q = K''(V+\phi)^{1-\gamma}. \qquad \ldots(3)$$

This can also be written as follows

$$V+\phi = K''Q^{1/1-\gamma}$$

or, if the term ϕ is neglected:

$$V = K''Q^{1/1-\gamma}. \qquad \ldots(4)$$

There are two possible circuit approaches, shown in Fig. 1.

In the first approach, referred to as the series configuration, the varactor is driven by a voltage source and produces a flow of charge in an output circuit. In this case, Eq.3 is most useful. In the second approach, referred to as the shunt configuration, the varactor is driven by a charge from a current source and produces a voltage which can be used in an output circuit.

In the case of an abrupt junction varactor Eq.4 becomes

$$V = K''Q^2. \qquad \ldots(5)$$

This means that an abrupt junction varactor in a shunt configuration will produce mainly the second harmonic of the input frequency. If the third harmonic of the angular input frequency ω is desired, it will be necessary to introduce a charge of 2ω from a so-called idler circuit and thus allow sum and difference frequencies to be produced. The idler circuit should be lossless and the idler charge included in the total Q in Eq.4 or 5. The sum frequency is the desired third harmonic output frequency. The difference frequency is the same as the input frequency and modifies the input impedance of the circuit.

If the varactor were a pure non-linear capacitor, there would be no losses and the efficiency would only be limited by circuit losses. The actual device has, however, a series resistance in the order of 1Ω or less. This resistance causes losses due to the total current through the device. The additional losses of the idler circuit are therefore one reason why a trebler has a lower efficiency than a doubler. Another reason is that, in general, the required input current increases with higher order harmonics.

The varactor series resistance is therefore an important characteristic of the device. This means that a varactor can be characterised by two curves: the series resistance R_s, usually measured at 400Mc/s or higher, and the small-signal capacitance C, usually measured at 100kc/s or 1Mc/s. Both characteristics must be given as a function of bias voltage. For the new BAY96 varactor, these curves are shown in Figs. 2 and 3.

Series resistance and capacitance together determine the cut-off frequency, which is usually defined as:

$$f_{co} = \frac{1}{2\pi R_s C}. \qquad \ldots(6)$$

The bias voltage at which f_{co} is specified is usually chosen near the breakdown voltage of the diode. The cut-off frequency is equal to the highest frequency at which the Q of the varactor can exceed 1.

CIRCUIT CONSIDERATIONS

It has been mentioned that there are two different circuit approaches: the series and the shunt configuration. Of these two the shunt configuration is more suitable for high-power harmonic generation for several reasons:

(i) The varactor is a relatively low-impedance device and therefore operates easier in a configuration that requires a low-impedance coupling element between input and output circuits.

(ii) The device can be grounded on one side, thus providing a good heatsink with the chassis.

(iii) Since the series resistance increases with temperature, a lower temperature due to better heatsinking means better efficiency.

The shunt configuration consists of a parallel connection of the varactor, the input and output matching networks, and one or more idler circuits.

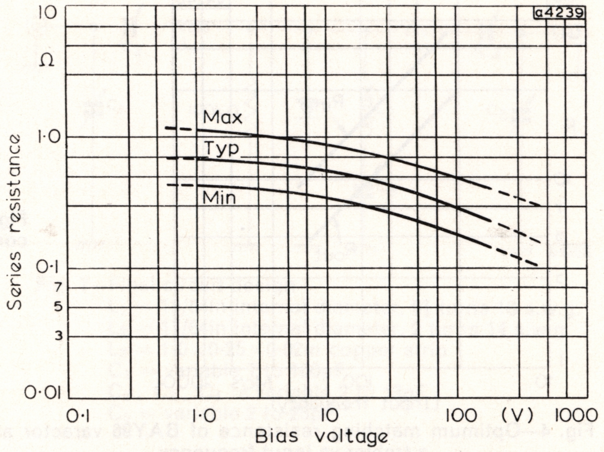

Fig. 2—Series resistance vs bias voltage (values obtained with early samples)

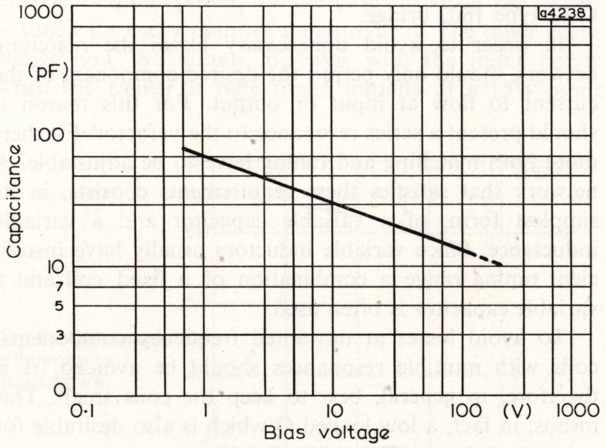

Fig. 3—Capacitance vs bias voltage at 1Mc/s (values obtained with early samples)

The function of the matching networks is dual, providing impedance matching while at the same time filtering spurious signals. Usually either double-tuned or single-tuned circuits are used. The design of the single-tuned circuits is much simpler but their spurious response is usually unacceptable. The double-tuned circuits will, in most cases, provide adequate suppression of spurious response, but it is difficult to design them for adjustable matching. An external input filter is usually not necessary.

Design and adjustment of the matching networks is complicated by the non-linear nature of the varactor. For every value of source resistance, there is a load resistance that will give the best efficiency; and conversely, for every load resistance, there is a source resistance value that will give the best efficiency. A certain combination of source and load resistances will give the maximum efficiency.

Penfield and Rafuse (Ref. 1) have calculated the optimum input and output matching resistances for abrupt junction varactor harmonic multiplier circuits. Their design curves, however, are based on operation in the reverse direction only, while in actual circuits the varactor is also driven in the forward direction. In addition, the varactor is not an ideal abrupt junction diode. However, measurements on actual triplers have shown that these curves can be quite useful for an initial design. The graph shown in Fig. 4 is based on these curves. It presents the optimum matching resistances for the BAY96 in tripler circuits as a function of the input frequency. The numerical scale

---

This article appeared originally in **Amperex Tech News**, Vol. 6, No. 1, March 1965.

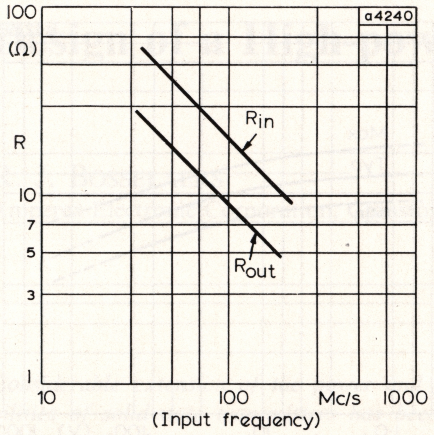

Fig. 4—Optimum matching resistance of BAY96 varactor as a trebler vs input frequency

values are based on small-signal parameter measurements and are confirmed by impedance measurements using the G.R. type 1607 bridge.

In order to avoid unnecessary losses the matching network should only permit the desired component of the current to flow at input or output. For this reason it should present a series resonance to the varactor. Furthermore both matching and tuning have to be adjustable. A network that satisfies these requirements consists, in its simplest form, of a variable capacitor and a variable inductance. Since variable inductors usually have insufficient tuning range a combination of a fixed coil and a variable capacitor is often used.

To avoid losses at unwanted frequency components, coils with multiple resonances should be avoided. It is therefore, in general, best to keep the coils small. This means, in fact, a low loaded Q which is also desirable for reasons of circuit efficiency.

DESIGN OF MATCHING NETWORKS

The requirements for the matching networks have been discussed extensively in the previous paragraph. A typical example of such a network is shown in Fig. 5. The resistance R_o represents either source or load resistance. Variable matching is obtained by means of C_1.

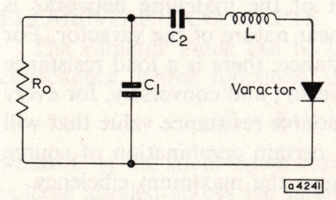

Fig. 5—Typical matching network

The series equivalent resistance of the R_o-C_1 combination should match the optimum resistance for the varactor which can be estimated from Fig. 4 for the BAY96. Any series-parallel conversion chart can be used to determine the required value of C_1. One that is particularly useful in this case and which can easily be constructed on log-log paper is shown in Fig. 6. It is based on the following relation:

$$\left(\frac{X_p}{R_p}\right)^2=\left(\frac{R_s}{X_s}\right)^2=\frac{R_s}{R_p-R_s} \qquad \ldots(7)$$

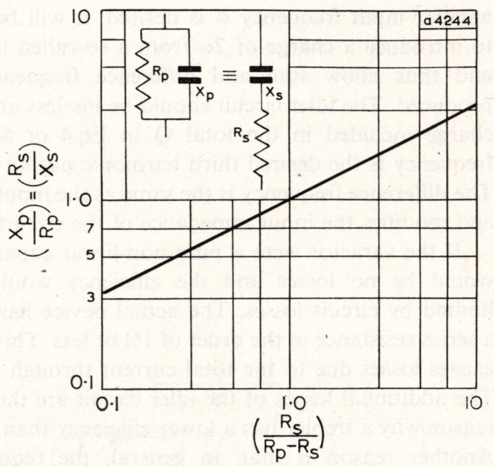

Fig. 6—Series-parallel conversion chart

where R_p is the known source or load resistance (usually 50Ω), R_s is the desired matching resistance, X_p is the reactance of C_1 (to be determined), and X_s is useful for the determination of C_2.

The value of L can be determined from the desired loaded Q of the circuit. Usually Q = 3 to 10 for a good design.

EXAMPLE

It is required to design the matching network for a 150 to 450Mc/s trebler using the BAY96. Source and load resistance are both 50Ω.

Input Network

From Fig. 4 we find that the desired matching resistance is equal to $R_{in} = 13\Omega$.

The reactance of C_1 can be found from Fig. 6; where for a value on the abscissa of

$$\frac{R_{in}}{R_g-R_{in}}=\frac{13}{50-13}=0{\cdot}35$$

the ordinate value is equal to

$$X_{C1}/R_g = 0{\cdot}59 \quad \text{or} \quad X_{C1} = 29{\cdot}5\Omega \quad \text{and} \quad C_1 = 35\text{pF}.$$

The inductance can be found from the loaded Q. For Q = 10

$$X_{L1} = 20 \text{ times } R_{in} = 260\Omega.$$

This is equivalent to −4·1pF. The total tuning capacitance is therefore 4·1pF. The equivalent capacitance of the R_g-C_1 combination can be calculated from the value of R_s/X_s on the chart (Fig. 6):

$$R_{in}/X_s = 0{\cdot}59 \quad \text{or} \quad X_s = 22\Omega.$$

This corresponds with 49pF. The required value of C_2 depends on the effective input capacitance of the varactor. Since the observed values (45pF and higher) are not consistent with predictions, it is best to choose the range of C_2 with sufficient margin. With C_{in} = 45pF the value of C_2 becomes

$$C_2=\frac{1}{\frac{1}{4{\cdot}1}-\frac{1}{49}-\frac{1}{45}}=5\text{pF}.$$

Output Network

From Fig. 4 we find that the desired output matching resistance is

$$R_o = 6\Omega \quad \text{and} \quad \frac{R_o}{R_L-R_o}=\frac{6}{50-6}=0{\cdot}136.$$

Fig. 6 gives

$$X_p/R_p = R_s/X_s = 0{\cdot}37.$$

So

$$X_{C5} = 18{\cdot}5\Omega \quad \text{or} \quad C_5 \text{ (Fig. 7)} = 19\text{pF}.$$

Again using Q = 10

$$X_{L3} = 20R_o = 120\Omega.$$

This is equivalent to −3pF.

The equivalent reactance of the R_o-C_4 combination is:

$$X_s=\frac{6}{0{\cdot}37}=16{\cdot}2\Omega.$$

This corresponds with 22pF.

The effective output capacitance of the varactor also shows no correlation with predicted values. The lowest observed value is approximately 18pF. Using this value to calculate C_4 we find:

$$C_4=\frac{1}{\frac{1}{3}-\frac{1}{22}-\frac{1}{18}}=4{\cdot}4\text{pF}.$$

Idler Circuit

The idler circuit should tune at 300Mc/s and the equivalent series loss resistance should preferably be equal to or smaller than the varactor series resistance.

Assuming $R_s = 0{\cdot}5\Omega$ and Q = 100 we find

$$1/\omega C = 50\Omega \quad \text{or} \quad C_3 = 10\text{pF}.$$

Results

A circuit was constructed according to the design example. Details of the circuit are given in Fig. 7. The circuit was used in combination with a 450Mc/s fixed bandpass filter. The obtainable efficiency at each level of input power is shown in Fig. 8. To illustrate the ease of tuning, two curves are given in Fig. 10. One curve shows output vs input power for the case in which the trebler is tuned for every point of measurement. The other curve shows how the output increases with the input power when the trebler is only tuned initially at a 15W input

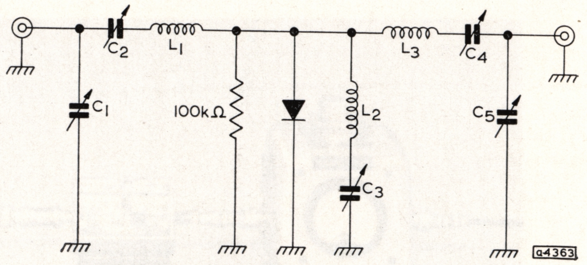

Fig. 7—Final circuit design
L_1 = 19/64in internal diameter, 6½ turns 18 s.w.g.
L_2 = 17/64in internal diameter, 2 turns 14 s.w.g.
L_3 = 1·0×0·25×0·02in copper strip
C_1 = variable 7 to 100pF
C_2, C_3, C_4 = variable 2 to 13pF
C_5 = variable 2 to 25pF

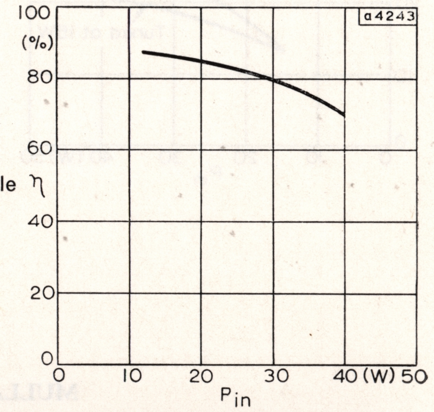

Fig. 8—Obtainable efficiency vs input power

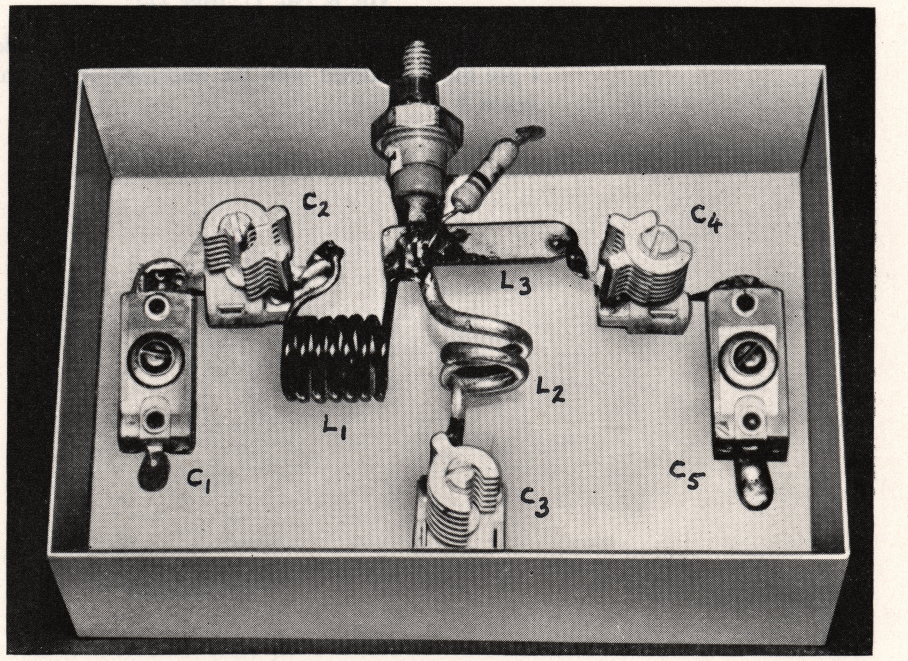

Fig. 9—Varactor tripler

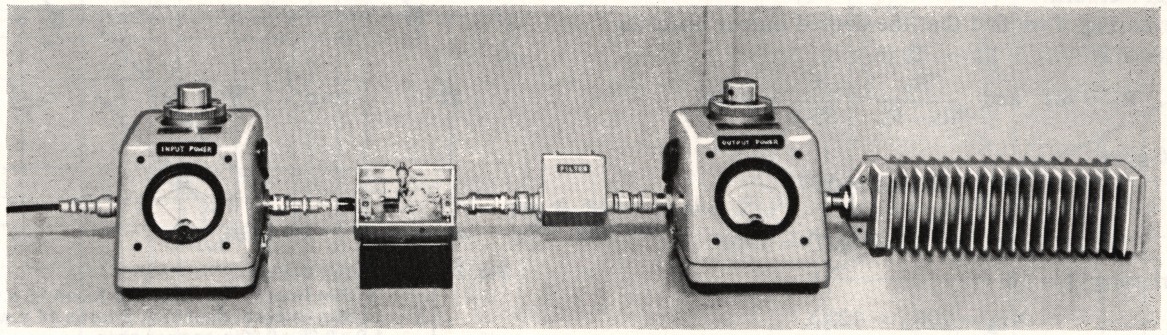

Fig. 11—Varactor trebler in test circuit

level. This plot shows that the trebler will give 75% of its full output power when the input is raised from 15W to 40W without retuning. Tuning at the 40W level can then be accomplished in a time short enough to ensure that no damage will occur to components when the transmitter is intended for intermittent operation only.

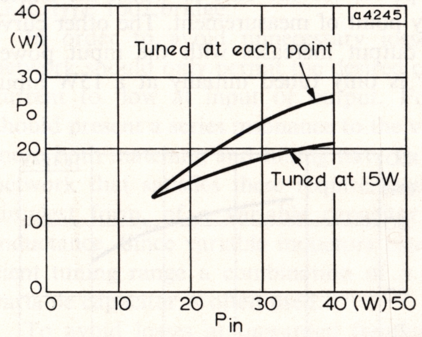

Fig. 10—Output vs input power

ACKNOWLEDGEMENT

The author wishes to thank R. J. Kufel for the construction of the trebler, for the measurements, for the experimental data on which the design curve is based, and for useful suggestions regarding the article.

REFERENCES

1. Penfield, P., and Rafuse, R. P. 'Varactor Applications'. M.I.T. Press, 1962.
2. Kaylie, H. L. 'The Design of Varactor Frequency Multipliers for Mobile Communications'. I.E.E.E. Vehicular Communications Conference, Dallas, 1963.

MULLARD TECHNICAL COMMUNICATIONS

Vol. 8, No. 77, page 227

The values quoted for Magnadur grade 'X' in Table 1 are those obtained with the improved version of grade 3.